ISPRS Journal of Photogrammetry and Remote Sensing 69 (2012) 146–166

Contents lists available at SciVerse ScienceDirect

ISPRS Journal of Photogrammetry and Remote Sensing

journal homepage: www.elsevier.com/locate/isprsjprs

Potential of texture measurements of two-date dual polarization PALSAR data for the improvement of forest biomass estimation

Md. Latifur Rahman Sarker [a,d,*], Janet Nichol [b], Baharin Ahmad [a], Ibrahim Busu [a], Alias Abdul Rahman [c]

[a] Department of Remote Sensing, Universiti Teknology Malaysia, Malaysia
[b] Department of Land Surveying and Geo-Informatics, The Hong Kong Polytechnic University, Hong Kong
[c] Department of Geoinformatics, Universiti Teknology Malaysia, Malaysia
[d] Department of Geography & Environmental Studies, University of Rajshahi, Bangladesh

ARTICLE INFO

Article history:
Received 16 November 2009
Received in revised form 3 February 2012
Accepted 1 March 2012
Available online 10 April 2012

Keywords:
PALSAR
Dual polarization
SAR image texture
Saturation level
Forest biomass
Leave-One-Out Cross-Validation

ABSTRACT

The recently available space-borne SAR sensor, PALSAR, is more promising than its predecessor JERS-1 for biomass estimation because of its long wavelength (L-band), and its ability to provide data with different polarizations, varying incidence angles and higher spatial resolutions. This research investigates the potential of two-date dual polarization (HH and HV) SAR imagery for biomass estimation using different kinds of texture processing and different combinations of single and dual polarization ratios. The investigation is conducted in a mountainous, sub-tropical study area where biomass levels are far beyond the previously recognized saturation levels for L-band SAR images, and forest is a mixture of native and non-native species and plantations.

We analyzed two-date SAR data with four steps of image processing, including raw data processing in various combinations, texture measurement parameters of HH and HV polarizations, texture measurement parameters of HH and HV together (both jointly and as a ratio), and a ratio of two-date texture parameters along with a single and two-date ratio. When the processed images were compared with ground data from 50 plots, the performance from raw data processing was low, with adjusted $r^2 = 0.22$, but after all four processing steps, promising model accuracy (adjusted $r^2 = 0.90$ and RMSE = 28.58 t/ha) and validation accuracy (using the Leave-One-Out-Cross-Validation) with adjusted $r^2 = 0.88$ and RMSE = 35.69 t/ha, were achieved from the combination of single- and two-date polarization ratios of texture parameters.

The strong performance achieved indicates that L-band dual-polarization (HH and HV) SAR data from PALSAR has great potential for biomass estimation, far beyond the previously reported L-band saturation point for biomass. This result is attributed to the synergy among texture processing and dual polarization on the one hand, which were able to average out random speckle noise, and the use of ratio instead of absolute quantities, due to its well known ability to reduce forest structural and terrain effects. The additional use of two-date SAR data with these processing techniques was able to add complementary information derived from biomass response in both wet and dry seasons. Thus overall, undesirable image noise and terrain effects were reduced.

1. Introduction

The estimation of forest biomass is one of the most persistent uncertainties in understanding the carbon cycle. This is especially true in tropical forest because of its complicated stand structure and species heterogeneity (Lucas et al., 2000; Nelson et al., 2000; Steininger, 2000; Foody et al., 2003; Lu, 2005, 2006). Remote sensing data, properly linked to forest biophysical properties, can address this problem (Harrell et al., 1995) by offering an effective method for forest biomass estimation at local, regional and global scales (Brown et al., 1989; Le Toan et al., 1992; Rosenqvist et al., 2003; Foody et al., 2003).

The most promising type of sensor appears to be Synthetic Aperture Radar (SAR) due to its sensitivity to forest structure (Harrell et al., 1995; Castel et al., 2002) as well as all-weather capability, and useful relationships have been established between radar backscatter and forest biophysical parameters (Dobson et al., 1992; Le Toan et al., 1992). Many studies of biomass have been conducted using both airborne (Wu, 1987; Le Toan et al., 1992; Dobson et al., 1992; Ranson and Sun, 1994; Ranson et al., 1995;

* Corresponding author at: Department of Remote Sensing, Universiti Teknology Malaysia, Malaysia. Tel.: +60 11 15158825; fax: +60 7 5566163.
E-mail address: lrsarker@yahoo.com (Md. Latifur Rahman Sarker).

0924-2716/$ - see front matter © 2012 International Society for Photogrammetry and Remote Sensing, Inc. (ISPRS) Published by Elsevier B.V. All rights reserved.
http://dx.doi.org/10.1016/j.isprsjprs.2012.03.002

Dobson et al., 1995; Kasischke et al., 1995; Foody et al., 1997; Harrell et al., 1997; Luckman et al., 1997; Mougin et al., 1999; Santos et al., 2003) and space borne SAR (Luckman et al., 1998; Kurvonen et al., 1999; Fransson and Israelsson, 1999; Santos et al., 2002; Castel et al., 2002; Sun et al., 2002; Tsolmon et al., 2002; Kuplich et al., 2005; Lucas et al., 2007; Champion et al., 2008) and differing degrees of success have been obtained.

Most previous studies using space-borne SAR have been limited to single frequency and single polarization data. Although multi-polarization and multi-frequency airborne SAR has been used for biomass estimation, it has not been widely available or geographically extensive due to the lack of extensive and/or repeat data, though the results of these studies represent the foundation for most current and future SAR research (Townsend, 2002). Previous research recommends P-band SAR as the most suitable choice for measurement of woody biomass (Dobson et al., 1992; Le Toan et al., 1992; Rignot et al., 1994; Ranson and Sun, 1994; Kasischke et al., 1995; Imhoff, 1995; Harrell et al., 1997; Mougin et al., 1999; Kurvonen et al., 1999; Santos et al., 2003) but there is currently no space borne platform with P band radar. However, researchers also found L-band, particularly the cross polarized L-HV, to be effective for biomass estimation (Hussin et al., 1991; Le Toan et al., 1992; Dobson et al., 1992; Rignot et al., 1994; Ranson and Sun, 1994; Kasischke et al., 1995; Harrell et al., 1997; Luckman et al., 1997; Sun et al., 2002; Ranson et al., 1997; Lucas et al., 2007).

Until recently JERS-1 was the only Satellite SAR operating in L-band, but its single-band, single-polarization configuration was not optimal for forest biomass estimation (Townsend, 2002), and many researchers (Sun et al., 2002; Castel et al., 2002; Hese et al., 2005; Lucas et al., 2007) expected the new generation space borne SAR sensors particularly PALSAR to significantly improve biomass estimation. Currently the three most advanced satellite SAR sensors i.e. PALSAR (L-Band), RADARSAT-2 (C-Band) and TerraSAR (X-Band) provide data with different polarizations, different incidence angles and high spatial resolutions, and this has provided new opportunities for research in biomass estimation using SAR data.

However, the improvement of biomass estimation depends not only on the SAR data but also requires efficient SAR data processing (Imhoff, 1995), as the raw SAR backscattering coefficient becomes saturated at fairly low biomass levels (Kurvonen et al., 1999; Dobson et al., 1992; Kasischke et al., 1994; Rauste et al., 1994; Rignot et al., 1994; Foody et al., 1997). Several ways have been suggested to estimate biomass beyond the saturation point. These include (i) using longer wavelengths (Imhoff, 1995) due to their better canopy penetration than shorter wavelengths, enabling more backscatter from the woody components, (ii) using SAR data processing such as texture, as texture can maximize the discrimination of spatial information independently of tone (i.e. backscatter) and increase the biomass range that can be measured, thus increasing the saturation level (Kuplich et al., 2005; Luckman et al., 1997; Salas et al., 2002; Champion et al., 2008), (iii) using the ratio of SAR images, as polarization ratios do not saturate as quickly (Dobson et al., 1995). In addition, ratios can reduce topographic bias (Ranson et al., 2001; Ranson et al., 1995; Shi and Dozier, 1997), and forest structural effects (Foody et al., 1997; Dobson et al., 1995; Ranson et al., 1995; Ranson and Sun, 1994) and thus enhance the relationship between radar backscatter and biomass beyond observed saturation levels. Furthermore, it has been suggested to estimate biomass (iv) using several SAR images by averaging or other means, to reduce speckle induced error and other random errors in the estimation process (Kurvonen et al., 1999; Fransson and Israelsson, 1999). It therefore seems reasonable to expect that biomass estimation could be improved by using longer wavelength SAR data accompanied by different image processing techniques. This research takes into consideration recommendations from previous SAR biomass studies, in the context of newly available advanced SAR sensors and SAR processing algorithms.

1.1. Objectives

The main objective of this research is to investigate the potential of L-Band dual polarization SAR (PALSAR) data for biomass estimation in a complex sub-tropical evergreen forested region, where biomass levels are far beyond the previously stipulated saturation levels of L-band. Other more specific objectives are to

- investigate the performance of two-date raw SAR data using a variety of combinations of HH & HV polarization, both individually and jointly, for biomass estimation,
- explore the potential of texture parameters of HH & HV polarization SAR data for biomass estimation,
- investigate the potential for biomass estimation using HH & HV texture parameters both jointly (without ratio), and as ratio, and
- investigate the ratio of two-date dual polarization (HV & HH) texture parameters, along with a combination of single and two-date ratios for biomass estimation.

2. Study area and data

The study area for this research is the Hong Kong Special Administrative Region (Fig. 1) which lies on the southeast coast of China, just south of the Tropic of Cancer. The total land area of Hong Kong is 1100 km^2 and includes 235 small outlying islands. Although the population is over 7 million, only about 15% of the territory is built-up and less than 1% is still actively cultivated. Approximately 40% of the total area is designated as Country Parks which are reserved for forest succession under the management of the Agriculture, Fisheries and Conservation Department (AFCD). The native sub-tropical evergreen broad leaf forest has been replaced by a complex patchwork of regenerating secondary forest in various stages of development, and plantations. Forest grades into woodland, shrubland then grassland at higher elevations.

Two dates of images with dual polarization (HV and HH) from the L-band fine-beam PALSAR SAR sensor were used in this study (Table 1).

3. Methodology

The methodology (Fig. 2) of this study comprises two parts, i.e. allometric model development for field biomass estimation, and SAR image processing.

3.1. Allometric model development

Due to the lack of an allometric model for converting the measurable tree parameters to actual biomass, it was necessary to harvest and measure a representative sample of trees. Since tree species in Hong Kong are very diverse, the harvesting of a large sample was required. This was done by selecting the dominant tree species comprising a total of 75 trees in 4 DBH (diameter at breast height) classes (less than 10, 10–15, 15–20 and 20 cm and above) and standard procedures were followed for tree harvesting (Overman et al., 1994; Brown, 1997; Ketterings et al., 2001).

The harvested trees were separated into fractions including leaves, twigs, small branches, large branches, and stem. After measuring the fresh weight, representative samples (Fig. 3) from every part of the tree were taken for dry weight measurements in an oven at 80 °C until a constant dry weight was obtained (Fig. 3). The weight of every sample was estimated using the same electric

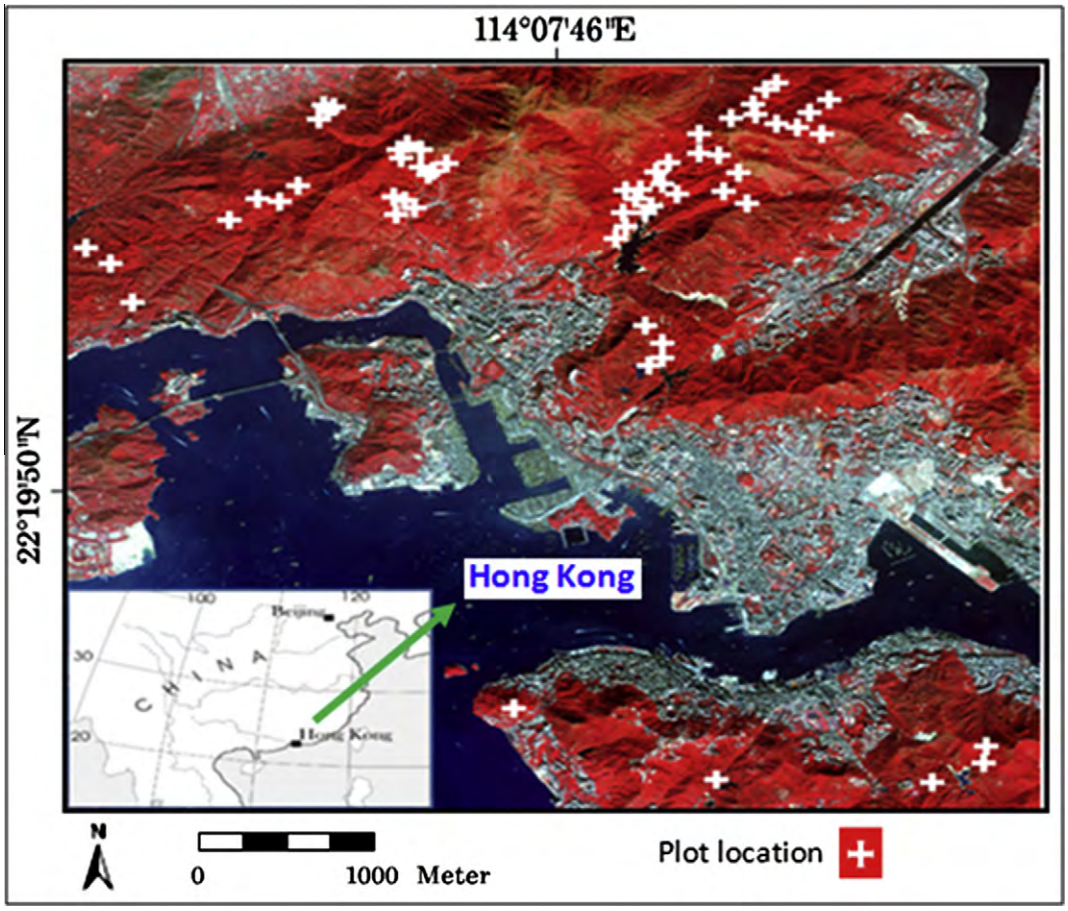

Fig. 1. Study area and location of the sample plots.

Table 1
PALSAR data description.

Date	26 September, 2008	11 May, 2008
Frequency Band	L-Band	L-Band
Mode	Ascending	Ascending
Polarization	HH + HV	HH + HV
Incidence angle	34.4	34.4
Product type	Ground range, 1.5 level	Ground range, 1.5 level
Pixel spacing	10 × 10	10 × 10

weight balance at 0.002 gm precision. The ratio of dry weight (DW) to fresh weight (FW) was calculated for every part of the samples using DW and FW of each part of the tree. Using the ratio, DW was calculated for every part, and finally the DW of each tree was calculated by summing the DW of all parts.

Regression models used by previous researchers (Brown et al., 1989; Overman et al., 1994; Arevalo et al., 2007) were tested in order to find the best fit using DW as the dependent variables and DBH and height as the independent variable in different combinations. Finally, using the log transformed DBH and dry weight (DW) the best fit model (Table 2) was found, considering all test parameters including correlation coefficient (r), coefficient of determination (r^2), the adjusted coefficient of determination (adjusted r^2), and RMSE. Approximately 93.2% accuracy (adjusted r^2 0.93) and RMSE 13.50 t/ha were obtained using this best fit model (Table 2). This was deemed highly satisfactory in view of the great variety of tree species, and is similar to the accuracies of several other studies (Brown et al., 1989; Overman et al., 1994).

3.2. Field plot measurement and field biomass estimation

To build a relationship between image parameters and field biomass, 50 sample plots covering a variety of tree stand types were selected after consultation with country park officers, using purposive sampling. Circular plots with a 15 m radius were determined considering the image resolution (approximately 10 m), orthorectification error and GPS positioning error. All sample plots were positioned within a homogenous area of forest, avoiding steep slopes and at least 15 m distant from other features such as roads, water-bodies and other infrastructure. A Leica GS5+ GPS was used to determine the center of each plot using DGP mode for accuracy within ±3 m. For precise position, a PDOP value below 4 was always attempted. Both DBH and tree height were measured for all trees within the circular plot region. The DBH of trees (Fig. 4) was measured at 1.3 m above ground and the heights of small and large trees were measured by Telescopic-5 and DIST pro4, respectively (Fig. 4). Trees with diameter below 2.5 cm DBH were not included. Finally using the measured parameter DBH, the biomass of each tree and biomass of all trees in a plot were estimated (Table 3) using the allometric model developed for this study area.

3.3. SAR data processing

3.3.1. Calculation of backscattering coefficient

Before texture measurement, the image was converted from an arbitary floating point number output by the SAR processor to a calibrated backscattering coefficient σ_0 in dB using the following equation:

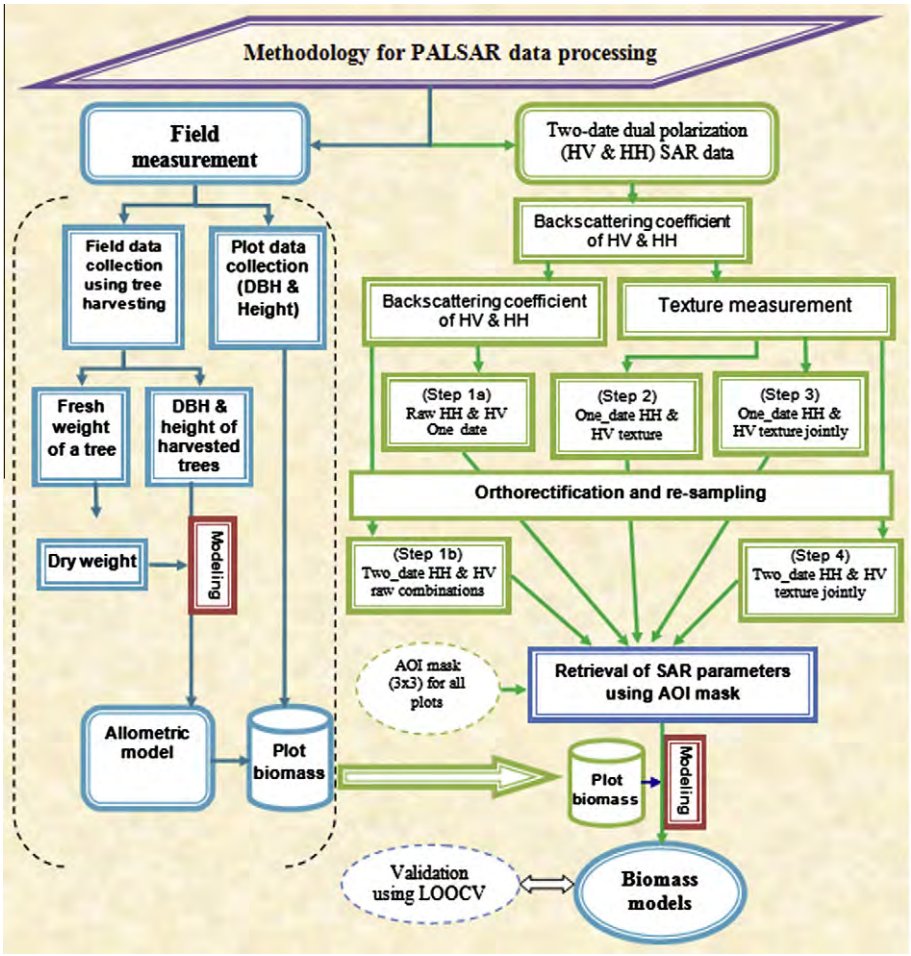

Fig. 2. Overall methodology.

Fig. 3. Tree harvesting procedure.

$$\sigma_0(\mathrm{dB}) = 10 \cdot \log_{10}(\mathrm{DN} \cdot \mathrm{DN}) - \mathrm{CF}$$

where DN = digital number, and CF = sensor calibrated constant, set at 83.0 dB. The σ_0 in dB was converted to σ_0 in power image and this was then converted to amplitude to use as an input to texture measurement, mainly because the amplitude image provides a better dynamic range over low backscattering targets. Subsequently, conversion to σ_0 in power and σ_0 in dB were carried out for model development.

3.3.2. Texture analysis

Texture is a characteristic used to identify objects or regions of interest in any image which is produced by spatial variations in image intensities (Baraldi and Parmiggiani, 1995) and studies have shown that in most cases, texture, not intensity, is the most important source of information in high-resolution radar images (e.g. Ulaby et al., 1986; Dobson et al., 1995; Podest and Saatchi, 2002; Dell'Acqua and Gamba, 2003). Several methods and techniques for describing texture, based on statistical models have been developed (Podest and Saatchi, 2002; Dekker, 2003; Kuplich and Curran, 2003; Kuplich et al., 2005). For this study, three categories of texture measurement were selected, to test their potential for biomass estimation (Table 4). The first is the grey level co-occurrence matrix (GLCM) (Haralick et al., 1973) along with some Grey Level Difference Vector (GLDV)-based texture measurements. The second is the sum and difference histogram proposed by Unser (1986) as an alternative to the usual co-occurrence matrices used. The third group is model based log form texture parameter estimation, reported by Oliver (1993) and Oliver and Quegan (2004). Extracting appropriate descriptions of texture also involves the selection of moving window sizes (Chen et al., 2004; Lu, 2005). In general a small window will produce noisier estimates of the texture descriptor but retain high spatial resolution, while a larger window will amplify estimation errors near spatial instationarities. However, the estimation of texture parameters should perhaps not

Table 2
Allometric model development.

Regression Model	Coefficient & Value		Std Err. of Coef.	Multiple r^2	r^2	Adjusted r^2	RMSE (kg)	p
In DW = $a + b *$ In DBH	a	-2.057	.183	.96	.93	93	13.52	.0005
	b	2.289	.072					

Fig. 4. Field plot measurement (DBH & Height).

Table 3
Dry weight (biomass) distribution of selected field plots.

Biomass range (t/ha)	Biomass of each plot	Number of plots	Percentage of plots
50–100	50.52, 57.45, 57.53, 61.14, 77.46, 78.11, 82.38, 83.24, 83.87, 92.16, 93.46, 94.68	12	24
100–150	104.60, 106.56, 107.04, 108.10, 109.39, 110.98, 111.67, 120.36, 122.96, 124.13, 131.55, 132.64, 133.07, 136.20, 138.04, 141.90, 147.49, 149.64	18	36
150–200	150.18, 151.46, 156.69, 157.44, 157.59, 163.14, 166.56, 168.02, 177.49, 178.49, 178.89, 188.62, 89.35	13	26
200–300	270.87	1	2
300 & above	312.05, 317.93, 346.09, 360.84, 518.60, 530.00	6	12
Total		50	100

use a fixed window at all because of the variation of the objects under investigation. Considering the need for texture measurement, the spatial resolution of the data (approximately 10 m) and that the forest structure in the study area is dense and compact, all texture measurements were performed using 5 small to medium window sizes from 3×3 to 11×11. Texture was computed based on directional invariant measures which are the averages among texture measures for four directions (0°, 45°, 90°, and 135°). Texture measurement was performed using the original data without speckle filtering because filtering averages out a lot of the texture characteristics. Although a good filtering algorithm suppresses speckle and preserves edges, these two requirements are hard to satisfy simultaneously, and there is always a trade-off between suppression of speckle and preservation of the detailed features, particularly texture (Nyoungu et al., 2002).

3.3.3. Geometric correction

Orthorectification of all texture images of two-date images was carried out using the Satellite Orbital Math Model to compensate distortions such as sensor geometry, satellite orbit and attitude variations, earth shape, earth rotation, and relief. To ensure effective co-registration between images all images were co-registered with a SPOT-5 image (as the reference image) and orthorectification was done using a high resolution (10 m) DEM and approximately 40 well distributed GCPs. For the date 1 image (26 September, 2008), the RMS error in X and Y was 0.32 and 0.22 pixels, respectively, while the overall error was 0.32 pixels. For date 2 image (11 May, 2008) the RMS error in X and Y was 0.24 and 0.24 pixels, respectively, while the overall error was 0.34 pixels. All images were resampled to a 10 m pixel size using nearest neighbor resampling.

3.4. Statistical analysis

To represent the relationship between field biomass and remotely sensed data, some researchers have used linear regression models with or without log transformation of field biomass data (Wu, 1987; Rauste et al., 1994; Ranson and Sun, 1994; Austin et al., 2003), while others have used multiple regression (Dobson et al., 1995; Kasischke et al., 1995; Rignot et al., 1995; Harrell et al., 1997; Mougin et al., 1999; Kurvonen et al., 1999; Townsend, 2002; Foody et al., 2003; Zheng et al., 2004; Hyde et al., 2006; Hyde et al., 2007). Non-linear regression (Santos et al., 2003) and semi-empirical models (Castel et al., 2002) have also been examined. Although no model can perfectly express this complex relationship, researchers are still using multiple regression models as one of the best choices. In this research, a stepwise, multiple-linear regression approach (Kutner et al., 2005) was used to establish relationships between the SAR parameters and field biomass collected from 50 plots.

An area of interest (AOI) mask representing an average of 3×3 pixels was used to extract quantities related directly to the σ_0 amplitude (referred to as SAR parameters hereafter) and SAR texture images (referred to as SAR texture parameters hereafter) from each sample plot. Retrieval of the mean value for each sample plot was conducted by overlaying the AOI mask on corresponding SAR image layers including (i) intensity of HH and HV polarizations along with the ratio of single date and two-date intensity data, (ii) texture images of HH & HV polarizations individually, iii) texture images of HH and HV jointly and as a ratio (HV/HH), and iv) the ratio of two-date HH & HV texture parameters along with single and two-date ratio combinations. All SAR image parameters were used as independent variables and the plot biomass (50 plots) as the dependent variable.

In multiple regression modeling, difficulties such as multicollinearity and overfitting may arise when a large number of independent variables are used, such that independent variables are highly correlated to one another. To avoid overfitting problems, as well as to ensure finding the best fit model, five common statistical parameters, namely correlation coefficient (r), coefficient of determination (r^2), adjusted r^2, RMSE and p-level (for the model) were computed. Another seven statistical parameters such as Beta coefficient (B), Std. Err. of B, p-level, tolerance (Tol = Tolarence = $1 - R_x^2$) , variance

Table 4
The formulas of texture measurements used in this study.

Gray level co-occurrence matrix (GLCM) based texture parameter estimation	Sum and difference histogram (SADH) based texture parameter	Model-based log form texture parameter estimation
1. Mean(ME) $= \sum_{i,j=0}^{N-1} iP_{i,j}$	1. Mean(μ) $= \frac{\sum_{ij} x_{ij}}{n}$	1.VI $= \frac{\sum_{ij} I_{i,j}^2}{\left[\frac{\sum_{i,j} I_{i,j}}{M}\right]^2} - 1$
2. Homogeneity (HO) $= \sum_{i,j=0}^{N-1} i \frac{P_{ij}}{1+(i-j)^2}$	2. Mean deviation(MD) $= \frac{\sum_{ij} \lvert x_{ij} - \mu \rvert}{n}$	2.VA $= \frac{\sum_{i,j} I_{i,j}}{\left[\frac{\sum_{i,j} A_{i,j}}{M}\right]^2} - 1$
3. Contrast (CO) $= \sum_{i,j=0}^{N-1} iP_{i,j}(i-j)^2$	3. Mean Euclidean distance(MED) $= \sqrt{\frac{\sum_{ij}(x_{ij} - x_1^2}{n-1}}$	3. VL $= \frac{\sum i,j \ln I_{i,j}^2}{M} - \left[\frac{\sum_{i,j} \ln I_{i,j}}{M}\right]^2$
4. Standard deviation (Std) $= \sqrt{\text{VA}}$ where VA $= \sum_{i,j=0}^{N-1} iP_{i,j}(i - \text{ME})^2$	4. Variance (σ^2) $= \frac{\sum_{ij}(x_{ij} - \mu)^2}{n-1}$	4. U $= \frac{\sum_{i,j} \ln I_{i,j}}{M} - ln\left[\frac{\sum_{i,j} I_{i,j}}{M}\right]$
5. Dissimilarity (DI) $= \sum_{i,j=0}^{N-1} iP_{i,j} \lvert i-j \rvert$	5. Normalised Coefficient of variation (NCV) $= \sqrt{\frac{\sigma^2}{\mu}}$	Here, I_i,j denotes the intensity of a pixel and A_i, j denotes the amplitude of a pixel
6. Entropy (EN) $= \sum_{i,j=0}^{N-1} iP_{i,j}(-\text{In}P_{ij})$	6. Skewness(sk) $= \frac{\sum_{ij}(x_{ij} - \mu)^3}{(n-1)\sigma^3}$	
7. Angula Second Moment (ASM) $= \sum_{i,j=0}^{N-1} iP_{i,j}^2$	7. Kurtosis(ku) $= \frac{\sum_{ij}(x_{ij} - \mu)^4}{(n-1)\sigma^4}$	
8. Correlation (CR) $= \sum_{i,j=0}^{N-1} iP_{i,j}\left[\frac{(i-ME)(j-ME)}{\sqrt{VA_i VA_j}}\right]$	8.Energy(E) $= \sum_{i,j} x_{ij}^2$	
9. *Inverse* Difference (ID) $= \sum_{i,j=0}^{N-1} i \frac{P_{i,j}}{\lvert i-j \rvert^2}$	9. Entropy(H) $= -\sum_{i,j} p_{ij} \text{ln}(p_{ij})$, with $p_{i,j} = \frac{x_{i,j}}{\sum_{i,j} x_{ij}}$	
10. GLDV Angular Second Moment ($GASM$) $= \sum_{k=0}^{N-1} V_k^2$	Here, $x_{i,j}$ stands for the pixel (i, j) value of pixel in the kernel over which is summed, n for the number of pixels that is summed, x_z for the kernel's center pixel value, and $p_{i,j}$ for the normalized pixel value.	
11. GLDV Entropy (GEN) $= \sum_{k=0}^{N-1} V_k(-\text{In}V_k)$		
12. GLDV Mean(GME) $= \sum_{k=0}^{N-1} kV_k$		
13. GLDV Contrast(GCO) $= \sum_{k=0}^{N-1} k^2 V_k$		
Here, $P(i, j)$ is the normalized co-occurrence matrix such that SUM(i,j = 0, $N-1$) ($P(i, j)$) = 1. $V(k)$ is the normalized grey level difference vector $V(k)$ = SUM(i,j=0, $N-1$ and $\lvert i-j \rvert$ = k)$P(i,j)$		

inflation factor ($VIF = VIF_j = \frac{1}{1-R^2}$), Eigen value (EV), and condition index ($CI = k_j = \frac{\lambda_{max}}{\lambda_j} = 1, 2, \ldots, p$) were calculated to test intercept fitness and multicollinearity effects. To indicate multicollinearity problems, a tolerance value of less than 0.10 (Belsley, 1990), VIF value of greater than 10 (Belsley, 1990; Kutner et al., 2005; Douglas et al., 2006; Hyde et al., 2007), Eigen value close to zero (Douglas et al., 2006; Belsley et al., 1980), and condition index greater than 30 (Belsley et al., 1980; Belsley, 1990; Douglas et al., 2006) were used as determinants.

3.5. Processing of SAR data for modeling

The SAR data were processed in the following four steps for biomass modeling.

3.5.1. First processing step: raw data

In order to test the potential of raw SAR data, the following SAR derived parameters were used in the multiple regression models:

(a) SAR derived parameters of HH and HV polarization individually for each of the two image dates,
(b) SAR derived parameters of HH and HV jointly (i.e. all independent parameters together in the model) for each date,
(c) SAR derived parameters of HH and HV as a ratio for each date,
(d) SAR derived parameters of two-date as a ratio. i.e. $\frac{HV_{date_1(20080511)} + HV_{date_2(20080926)}}{HH_{date_1(20080511)} + HH_{date_2(20080926)}}$, and
(e) Combination of single and two-date ratios of SAR derived parameters, i.e.

joint intensity ratio-1) $\left[\frac{HV_{date_1(20080511)} + HV_{date_2(20080926)}}{HH_{date_1(20080511)} + HH_{date_2(20080926)}} \& \frac{HV_{date_1(20080926)}}{HH_{date_1(20080926)}}\right]$

and

joint intensity ratio- 2) $\left[\frac{HV_{date_1(20080511)} + HV_{date_2(20080926)}}{HH_{date_1(20080511)} + HH_{date_2(20080926)}} \& \frac{HV_{date_1(20080511)}}{HH_{date_1(20080511)}}\right]$.

3.5.2. Second processing step: with texture

One hundred and twenty five texture parameters derived in HH as well as HV polarization, using 25 texture measurements, from five window sizes were used in the modeling as follows:

(a) All 125 parameters derived from HH texture measurements individually for each date, and
(b) All 125 parameters derived from HV texture measurements individually for each date.

3.5.3. Third processing step: texture with both polarizations

Since the result of the previous step (step-2) revealed that neither HH nor HV polarization texture parameters alone produce a satisfactory model for biomass in this high biomass situation, we then tested for improvement, using texture parameters of HH & HV polarizations together in the modeling as follows:

(a) Texture parameters from HH and HV polarizations jointly for each date, i.e. 250 texture parameters (125 from each polarization) from both polarizations were used in the modeling, and
(b) Texture parameters from HH and HV polarizations as a ratio for each date, i.e. the ratio of 125 texture parameters (125 from each polarization) were used in the modeling.

3.5.4. Fourth processing step: two-date texture parameter combination

While in all previous texture processing steps the investigations were carried out using two-date images individually, here we used the ratio of two-date dual polarization texture parameters as independent variables in the modeling in order to take advantage of greater image averaging. This comprised:

(a) The ratio of texture parameters of two-date SAR data of both polarizations (125 independent variables), i.e. a two-date texture image ratio $= \frac{Texture\_HV_{date_1(20080511)} + Texture\_HV_{date_2(20080926)}}{Texture\_HH_{date_1(20080511)} + Texture\_HH_{date_2(20080926)}}$
(b) The combination of single and two-date ratios of texture derived SAR parameters (250 independent variables), i. e. joint texture ratio-1

$= \left[\frac{Texture\_HV_{date_1(20080511)} + Texture\_HV_{date_2(20080926)}}{Texture\_HH_{date_1(20080511)} + Texture\_HH_{date_2(20080926)}} \& \frac{Texture\_HV_{date_2(20080926)}}{Texture\_HH_{date_2(20080926)}}\right]$

Joint texture ratio-2

$= \left[\frac{Texture\_HV_{date_1(20080511)} + Texture\_HV_{date_2(0080926)}}{Texture\_HH_{date_1(20080511)} + Texture\_HH_{date_2(20080926)}} \& \frac{Texture\_HV_{date_1(20080511)}}{Texture\_HH_{date_1(20080511)}}\right]$.

3.6. Biomass estimation model validation

One important but at the same time difficult aspect of forest biomass estimation from remote sensing data is model validation. Validation is a useful and necessary part of the model building process in order to determine if the model will function successfully in its real world environment (Douglas et al., 2006). By far the preferred method to validate a regression model is through the collection of new data but the collection of new data is often neither practical nor feasible (Kutner et al., 2005). Thus, because of the scarcity of field biomass data, biomass estimation models have rarely been validated adequately (Lu, 2006).

In this research, data from 50 field plots were used to develop models and the number of field plots is considered reasonable and comparable or better than other similar studies. The use of some plots for model validation would leave fewer plots for model development, but the option was considered undesirable due to the large number of image parameters (as independent variables) used in this research as well as the possible omission of some valuable data from the model development process.

Therefore, considering the importance of model validation as well as the limited amount of field biomass data, this research performed cross-validation using the Leave-One-Out-Cross-Validation (LOOCV) method. Leave-One-Out Cross-Validation is a sensible choice as it has been shown to provide an almost unbiased estimate of the true generalization ability of models (Cawley and Talbot, 2004). For this method the model is trained multiple times, using all but one of the training set data points. The form of the LOOCV algorithm can be defined as follows:

For $k = 1$ to R (where R is the number of training set points)

- Temporarily remove the kth data point from the training set.
- Train the learning algorithm on the remaining $R - 1$ points.
- Test the removed data point and note your error.

Calculate the mean error over all R data points.

This model has not presently been applied to the validation of biomass estimation models although it has been used successfully in other disciplines such as neural network. The advantage of LOOCV for the validation of biomass estimation is that this process does not waste data and the resulting regression model is essentially the same as if it had been developed using all the data points. However, the main drawback to the LOOCV is that it is expensive – the computation must be repeated as many times as there are training set data points (Cawley and Talbot, 2004). Considering the field data points (50) and computational intensity of the LOOCV method, this validation was only conducted for the best three models proposed in Section 4.4.

4. Results and analysis

The biomass of the 50 field plots, which ranged from 55 to 530 t/ha, was used as the dependent variable and SAR parameters derived from different processing combinations of two-date dual polarized SAR data were used as independent variables in the modeling process. The results and analysis of the four processing steps are presented as four separate subsections.

4.1. Step 1: Biomass estimation using two-date raw PALSAR data

Forest biomass was estimated from raw SAR data using the method described in Section 3.5.1. In general, the relationships between field biomass and all raw SAR derived parameters were found to be poor, considering all 11 models tested (Figs. 5 and 6). In the first stage, a combination of HV and HH of date 2 (11 May, 2008) showed a stronger relationship (adjusted r^2=0.22) than date 1 (26 September, 2008), but was still too low to give sound biomass estimates. Similar poor results were also obtained from the second stage of analysis using the different types of two-date image ratios (Fig. 6).

The poor results obtained from the intensity data processing were not completely unexpected because of speckle noise and the known saturation problem of SAR data. Previous studies (Kurvonen et al., 1999; Dobson et al., 1992; Kasischke et al., 1994; Rauste et al., 1994; Rignot et al., 1994; Foody et al., 1997) have shown that direct application of the backscattering coefficient for biomass retrieval is limited by saturation unless the effects of forest structure are explicitly taken into account. Despite the problem of speckle noise and saturation level, many researchers found good relationships using the ratio of raw backscattering from different polarizations (Dobson et al., 1995; Ranson et al., 1995; Ranson and Sun, 1994; Harrell et al., 1997; Kasischke et al., 1997; Rignot et al., 1994; Mougin et al., 1999). Moreover, some researchers also found good results using a set of SAR images in the averaging process (Kurvonen et al., 1999; Townsend, 2002). However, in this research we obtained poor results for biomass estimation using all intensity data processing combinations (single-date ratio, two-date ratio, and single and two-date ratio) of SAR data.

This inconsistency with other studies can be explained by the fact that the biomass of our field plots is very high, with almost 75% of plots having biomass above 100 t/ha (Table 3). This is beyond the reported saturation levels of raw L-band SAR data, from previous studies of ca. 50–70 t/ha (Dobson et al., 1992; Imhoff, 1995; Le Toan et al., 1992). Since previous work has demonstrated the potential of biomass estimates from texture images (Luckman

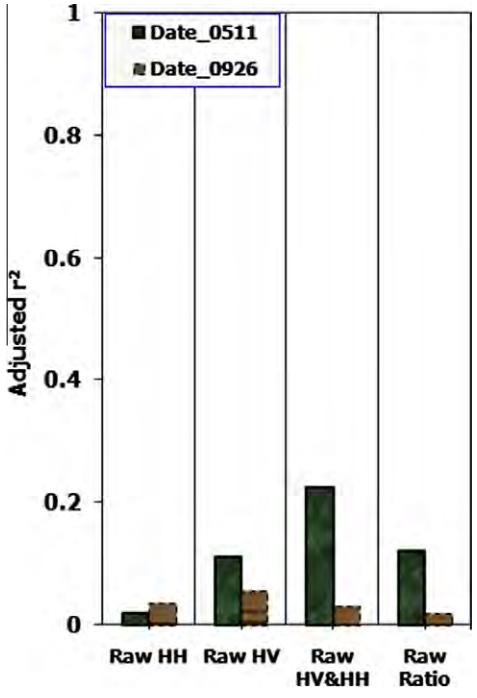

Fig. 5. Performance of biomass estimation using single date intensity data.

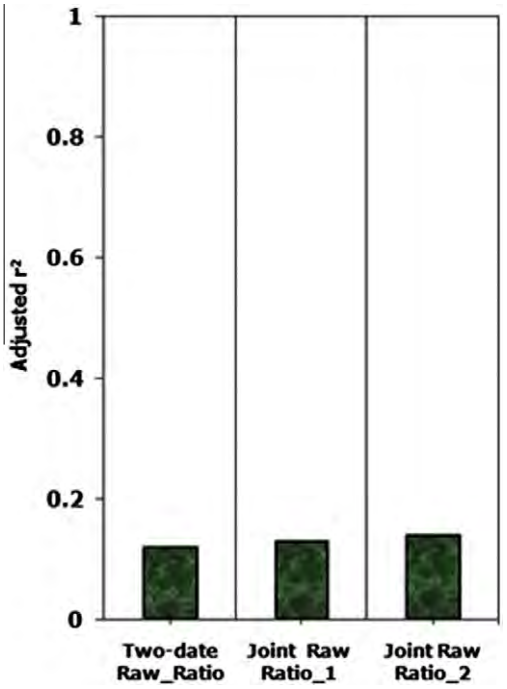

Fig. 6. Performance of biomass estimation using intensity data of two-date combination.

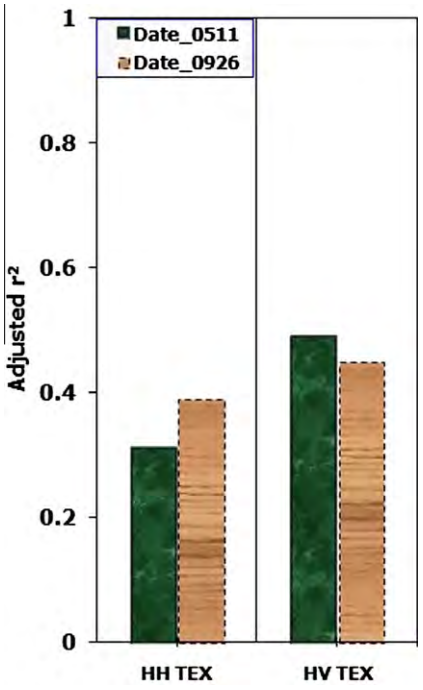

Fig. 7. Performance of biomass estimation using texture parameters of HH & HV polarizations.

Table 5
Results obtained from HH & HV dual polarization texture parameters.

Data	Model fitting parameters				Fitting parameters for intercept and variables							
	r^2	r^2_{adj}	RMSE (t/ha)	p-Level	Variable name & intercept	B	Std. Err. of B	p-Level	Tol	VIF	EV	CI
Model 1: Texture parameters of HH polarization (20080511)	0.35	0.31	74.60	.0001	Intercept	192.26	34.10	0.0005	–	–	3.20	1.00
					VI_HH_5×1764.60	−.08	369.44	0.0005	.12	8.31	.70	2.13
					Contrast_HH_3×3	−.08	.02	0.0001	.59	1.67	.08	6.09
					Normalized Coefficient of Variation_HH_7 × 7	−6402	1409	0.0005	.15	6.70	.01	17.29
Model 2: Texture parameters of HH polarization (20080926)	0.44	0.39	75.78	.0001	Intercept	327.12	50.62	0.0005	–	–	4.19	1.00
					Inverse_Difference_HH_5 × 5	−2191.04	420.19	0.0005	.18	5.43	.62	2.61
					GLDV Angular Second Moment_HH_9 × 9	4746.02	1087.53	0.0005	.56	1.78	.15	5.57
					Homogeneity_HH_3 × 3	−2191.04	196.49	0.0001	.25	4.01	.05	9.31
					Skewness_HH_9 × 9	−63.71	18.72	0.0001	.91	1.10	.01	19.98
Model 3: Texture parameters of HV polarization (20080511)	0.53	0 .49	69.09	.0000	Intercept	241.39	30.19	.00005	-	-	4.24	1.00
					Contrast_HV_5 × 5	2.1	0.37	0.0002	.13	7.93	.45	3.05
					Dissimilarity_HV_5 × 5	−52.0	12.09	0.0009	.09	11.05	.21	3.05
					VA_HV_11 × 11	−15613	4057	0.0003	.69	1.45	.08	7.22
					Contrast_HV_11 × 11	1.0	0.41	0.0190	.24	4.15	.02	16.12
Model 4: Texture parameters of HV polarization (20080926)	0.51	0 .45	71.16	.0005	Intercept	281	39.5	0.0005	–	–	4.820	1.00
					Normalized Coefficient of Variation_HV_11 × 11	−6830	1295	0.0004	.17	5.76	.81	2.42
					Dissimilarity_HV_11 × 11	29	10.2	0.0067	.31	3.20	.23	4.61
					Contrast_HV_3 × 3	−18	4.3	0.0009	.51	1.98	.08	7.76
					Variance_HV_11 × 11	3173224	872313	0.0007	.36	2.81	.05	10.15
					Standard Deviation_HV_9 × 9	49	15.8	0.0033	.14	7.27	.01	22.21

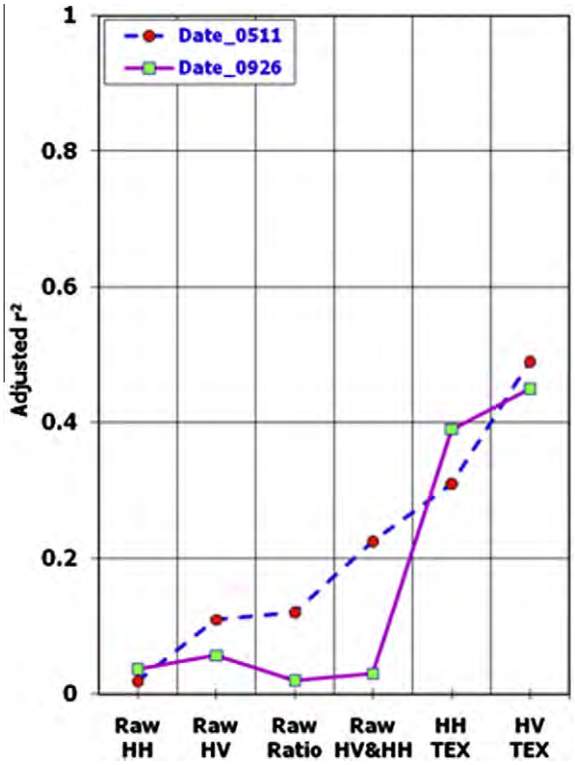

Fig. 8. Change in performance from intensity of HH & HV data to texture parameters of HH & HV.

et al., 1997; Salas et al., 2002; Kuplich et al., 2005; Champion et al., 2008), this research decided to investigate further using the SAR data processing technique of texture measurement.

4.2. Step 2: Biomass estimation using HH and HV texture parameters of two-date PALSAR data individually

The method described in Section 3.5.2 was used to estimate forest biomass from the texture parameters of SAR data. The result of biomass estimation improved substantially for both dates and for both polarizations using the texture parameters of HH & HV SAR data (Fig. 7 & Table 5), compared to all combinations of raw processing. The best results of 0.39 (adjusted r^2) and 0.49 (adjusted r^2) were obtained from the texture parameters of HH polarization (Model 2 in Table 5) and HV polarization (Model 3 in Table 5) data respectively. These results were 79.18% and 125.33%, higher (Fig. 8) than the best result (adjusted r^2=0.22) obtained from the raw data processing. The improved result using texture parameters is in agreement with the findings of previous studies (Luckman et al., 1997; Kuplich et al., 2005; Champion et al., 2008).

However, different results were obtained from the HH and HV texture parameters, with HV polarization (Fig. 7 and models 3 and 4 in Table 5) outperforming the HH polarization texture data (Fig. 7 and models 1 and 2 in Table 5). From the texture parameters of HH polarization the highest result (adjusted r^2 = 0.39 and RMSE = 75.78 t/ha) was obtained using model 2 (Table 5). This model used five texture variables (Inverse_difference_HH_5 × 5 + GLDV Angular Second Moment_HH_9 × 9 + Homogeneity_HH_3 × 3 + Skewness_HH_9 × 9). All variables were significant at the 95% significance level and multicollinearity effects were minimal. However only 40% of the variability was explained, and the estimated biomass of two high biomass plots was very far from the trend line (Fig. 9), thus yielding a very high RMSE (75.78 t/ha).

On the other hand, using the texture parameters of HV polarization the highest result (adjusted $r^2 = 0.49$) was obtained from model 3 (Table 5). This model only used four texture variables (Contrast_HV_5 × 5 + Dissimilarity_HV_5 × 5 + VA_HV_11 × 11 + Contrast_HV_11 × 11). Although all variables were significant and no multicollinearity effect was observed, only 50% of the variability is explained by this model, and the predicted biomass of some plots is still far from the trend lines (Fig. 10).

The better result obtained using the texture parameters of HV polarization rather than the texture parameters of HH polarization was not surprising, as this result confirms other studies which found HV polarization to have better sensitivity for biomass estimation (Rauste et al., 1994; Rignot et al., 1994; Dobson et al., 1995; Ranson et al., 1995; Kasischke et al., 1995; Mougin et al., 1999; Foody et al., 1997; Luckman et al., 1997; Collins et al., 2009). However, since we still obtained only ca. 50% variability of

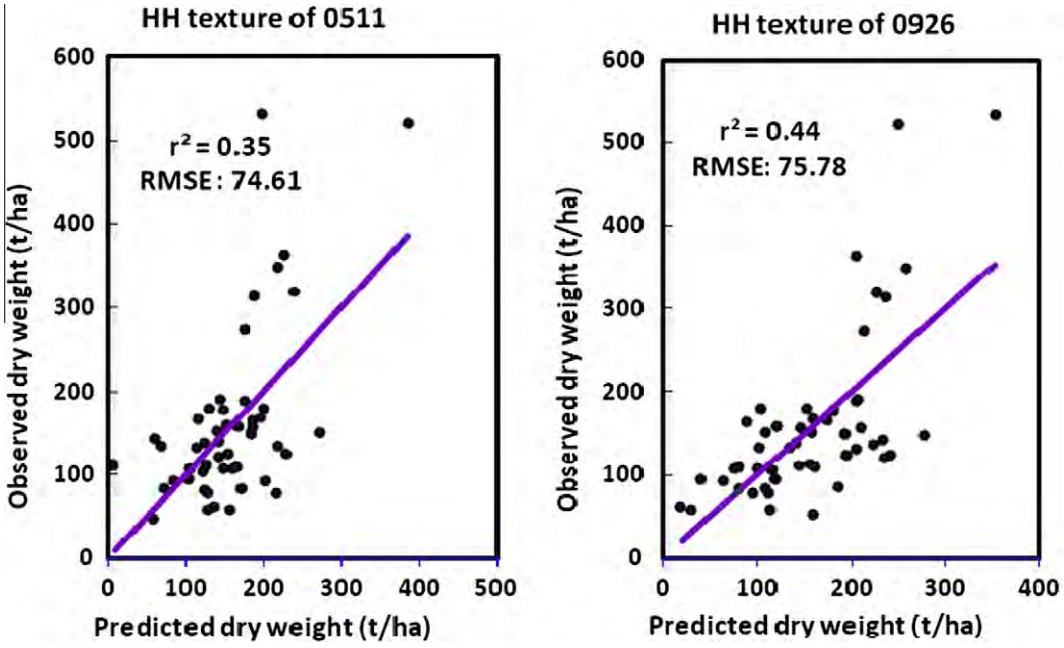

Fig. 9. Relationships between observed and model predicted biomass using texture parameters of HH polarization.

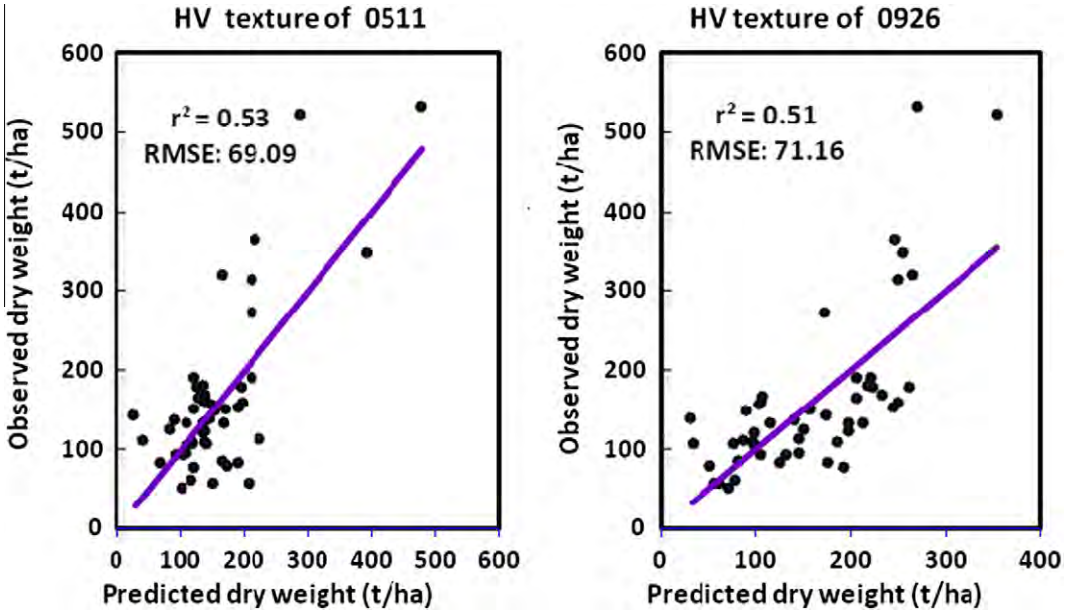

Fig. 10. Relationships between observed and model predicted biomass using texture parameters of HV polarization.

the field biomass using the texture parameters of HV polarization SAR data, we conclude, along with Ranson and Sun (1994), that both HH and HV polarizations alone are ineffective when biomass levels are beyond the normal saturation level of L-band SAR, as in our study area. As a result, we decided to explore further using both polarization SAR texture parameters together.

4.3. Step 3: Biomass estimation using combined HH and HV texture parameters of two-date PALSAR data

For the forest biomass estimation, the method depicted in Section 3.5.3 was developed using the HH and HV parameters jo intly (without and with ratio). The highest adjusted r^2 obtained were 0.63 and 0.78 (Table 6 and Fig. 11) using the HH and HV texture parameters jointly (without ratio), as well as the ratio (HV/HH) of texture parameters, respectively. This result indicates considerable improvement of biomass estimation (Fig. 12) compared to intensity (adjusted $r^2 = 0.22$, in Fig. 5), texture parameters of HH polarization (adjusted $r^2 = 0.39$, model 2 in Table 5) and texture parameters of HV polarization (adjusted $r^2 = 0.49$, model 3 in Table 5) data.

The best model using combined HH and HV texture parameters alone (without ratio) was found to be model 1 (Table 6), with six variables (Contrast_HV_5 × 5 + Normalized Coefficient of Variation_HH_11 × 11 + GLDV_Mean_HV_5 × 5 + Skewness_HH_7 × 7 + Dissimilarity_HV_11 × 11 + Kurtosis_HV_11×11). The model and intercept were significant and multicollinearity effects were not evident, as Tol, VIF and CI were less than the predefined thresholds. Although this model was significant and biomass estimation was improved compared to all previous processing steps (adjusted $r^2$0.63, Fig. 12), this model was not considered robust, with still only ca. 63% and relatively high RMSE (57.64 t/ha) due to some high biomass plots (Fig. 13). The better result obtained from the HH and HV polarization texture parameters together is not surprising as previous studies found that the use of multi-polarization datasets with both like- and cross-polarized channels can provide more information than either alone, and may improve biomass estimation algorithms (Ranson and Sun, 1994; Kasischke et al., 1997).

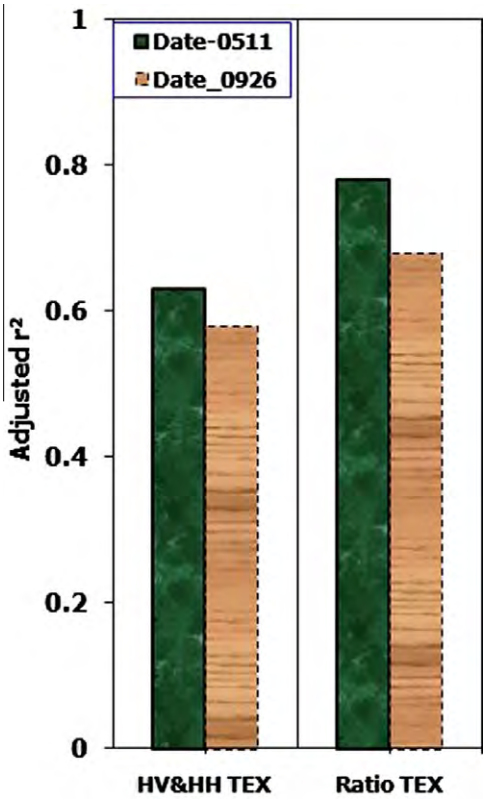

Fig. 11. Performance of biomass estimation using texture parameters of HH & HV polarizations together.

The best overall model (model 3 in Table 6) was obtained using the ratio of HV and HH polarization texture parameters with nine variables (Amplitude Image + Kurtosis_5 × 5 + Homogeneity_5 × 5 + Contrast_5 × 5 + Standard Deviation_3 × 3 + Angular Second Moment_9 × 9 + GLDV Angular Second Moment_11 × 11 + Variance_9 × 9 + VI_5 × 5). The performance of this model (adjusted $r^2 = 0.78$) was higher than that of all previous steps

Table 6
Results obtained from HH & HV dual polarization together.

Data	Model fitting parameters				Fitting parameters for intercept and variables							
	r^2	r^2_{adj}	RMSE (t/ha)	p-Level	Variables name & intercept	B	Std. Err. of B	p-Level	Tol	VIF	EV	CI
Model 1: Texture parameters of HV&HH (20080511)	0.67	0.63	57.64	.0005	Intercept	350.70	37.78	.00005			5.69	1.00
					Contrast_HV_5 × 5	2.06	0.32	0.0005	0.13	7.89	0.64	2.97
					Normalized Coefficient of Variation_HH_11 × 11	−2318.37	430.21	0.0003	0.81	1.24	0.36	3.97
					GLDV_Mean_HV_5 × 5	−51.84	10.17	0.0007	0.09	10.73	0.14	6.38
					Skewness_HH_7 × 7	59.97	24.23	0.0173	0.90	1.11	0.09	7.81
					Dissimilarity _HV_11 × 11	0.88	0.33	0.0110	0.27	3.78	0.06	10.09
					Kurtosis_HV_11 × 11	−3.20	1.49	0.0374	0.83	1.20	0.02	19.01
Model 2: Texture parameters of HV&HH (20080926)	0.64	0.58	60.62	.0005	Intercept	228.00	70.30	0.0023			6.39	1.00
					VL_HH_11 × 11	−293.71	100.89	0.0057	0.88	1.14	0.64	3.16
					Inverse_Difference_HH_5 × 5	−1812.98	356.38	0.0008	0.18	5.70	0.53	3.47
					GLDV Angular Second Moment_HH_9 × 9	5338	1020	0.0005	0.44	2.30	0.22	5.37
					Homogeneity_HH_3 × 3	543.08	170.22	0.0026	0.23	4.39	0.10	7.92
					Dissimilarity_HV_11 × 11	33.48	7.81	0.0001	0.40	2.48	0.09	8.45
					GLDV_Mean_HV_3 × 3	−13.70	3.56	0.0004	0.55	1.82	0.02	20.66
					Skewness_HH_7 × 7	−39.81	19.65	0.0491	0.94	1.07	0.01	25.47
Model 3: Ratio of single date texture parameters (20080511)	0.82	0.78	42.77	.0005	Intercept	698.66	62.91	0.0005			5.59	1.00
					Amplitude Image	-672.02	83.58	0.0005	0.49	2.05	1.86	1.73
					Kurtosis_5 × 5	−20.67	3.40	0.0005	0.76	1.33	1.06	2.30
					Homogeneity_5 × 5	28.07	4.28	0.0005	0.29	3.45	0.74	2.75
					Contrast_5 × 5	31.27	3.39	0.0005	0.15	6.81	0.34	4.05
					Standard Deviation_3 × 3	−23.72	5.82	0.0002	0.13	7.67	0.20	0.20
					Angular Second Moment_9 × 9	83.06	14.87	0.0002	0.12	8.46	0.14	6.36
					GLDV Angular Second Moment_11 × 11	−84.28	17.33	0.0018	0.12	8.17	0.04	12.71
					Variance_9 × 9	11.96	3.21	0.0006	0.42	2.40	0.03	14.88
					VI_5 × 5	−15.07	6.50	0.0255	0.26	3.81	0.01	27.67
Model 4: Ratio of single date texture parameters (20080926)	0.74	0.68	60.8	.0005	Intercept	5.090	.298	0.0000			3.04	1.00
					Sigma_dB	−0.30	0.12	0.0159	0.81	1.24	0.69	3.59
					Mean Dev. from mean_5 × 5	−3.17	0.44	0.0005	0.19	5.27	0.62	3.80
					Mean Euclidean Distance _7 × 7	4.20	0.67	0.0005	0.06	17.16	0.45	4.43
					Mean Euclidean Distance _11 × 11	−3.91	0.70	0.0002	0.06	16.04	0.15	7.58
					Variance_11 × 11	3.18	0.98	0.0024	0.17	5.93	0.10	9.54
					Kurtosis_11 × 11	−0.13	0.03	0.0003	0.71	1.41	0.05	13.06
					VI_9 × 9	0.73	0.20	0.0006	0.27	3.66	0.04	15.68
					Angular Second Moment_3 × 3	0.11	0.04	0.0060	0.82	1.22	0.02	19.23
					Standard Deviation_5 × 5	0.72	0.22	0.0018	0.20	5.09	0.01	25.23
					GLDV_Mean_5 × 5	−0.42	0.13	0.0017	0.20	5.02	0.01	35.62

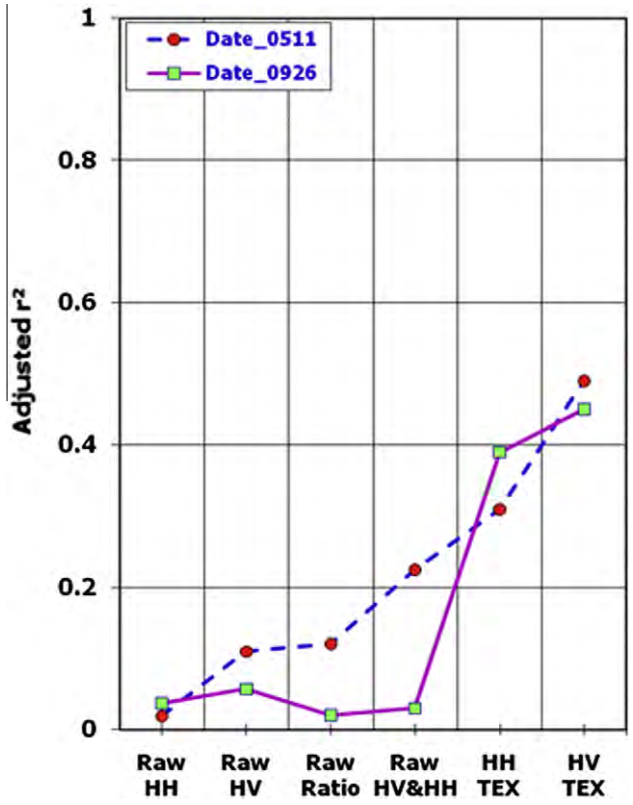

Fig. 12. Change in performance of biomass estimation from intensity of HH & HV polarizations to HH & HV texture parameters individually and jointly (without and with ratio).

including the use of HH and HV polarization texture parameters together (Fig. 12). The model and intercept were significant and multicollinearity effects were not significant according to the thresholds set for the multicollinearity assessment. The relationship between observed and model predicted biomass (Fig. 14) indicated that the model was robust and only a few plots deviated from the trend lines, giving a much lower RMSE of 42.77 t/ha. The improvement of biomass estimation using the ratio of dual polarization texture parameters is in agreement with previous studies in principle (Foody et al., 1997; Ranson et al., 1995; Dobson et al., 1995; Harrell et al., 1997; Shi and Dozier, 1997) which found that ratios of polarizations or bands have advantages for biomass estimation as polarization ratios do not saturate as quickly as single polarization. Moreover, ratios are known to reduce topographic effects (Ranson et al., 2001) which are considerable in our mountainous study area, and to reduce forest structural effects due to forest type (Foody et al., 1997; Dobson et al., 1995; Ranson et al., 1995). We believe that the model using the ratio of dual polarization texture parameters enhanced the relationship between radar backscatter and biomass by reducing the topographic effect and forest structural effect reasonably and effectively.

Although the result is promising, still only 78% variability of field biomass was obtained from this processing. However, up to this stage only single-date image ratios of dual polarization (HH and HV) SAR have been tested individually. Since previous studies have reported increased accuracy using more than one date of SAR images (Kurvonen et al., 1999), we decided to investigate a two-date ratio and two-date averaging of texture parameters for further improvement.

4.4. Step 4: Biomass estimation using different types of ratio of two-date PALSAR data jointly

The method illustrated in Section 3.5.4 for forest biomass estimation using the texture parameter ratio of two-date PALSAR data was tested. Compared to all previous image processing steps (Fig. 16), the performance (Fig. 15) of biomass estimation improved significantly using the two-date texture image ratio (Fig. 15 and model 1 in Table 7) and a combination of single and two-date texture image ratios (Fig. 15 and models 2 and 3 in Table 7).

Using the two-date ratio of dual polarization (HH and HV) texture parameters, the adjusted $r^2$was 0.83 (model 1 in Table 7 and Fig. 16) with nine variables Kurtosis_3x3p + Aplitude image_p + Skewness_5 × 5p + Homogeneity_5 × 5p + VI_11 × 11p + Skewness_11 × 11p + Kurtosis_11 × 11p + Angular Second Moment_5 ×5p + GLDV Entropy_3 × 3p). This result was considerably

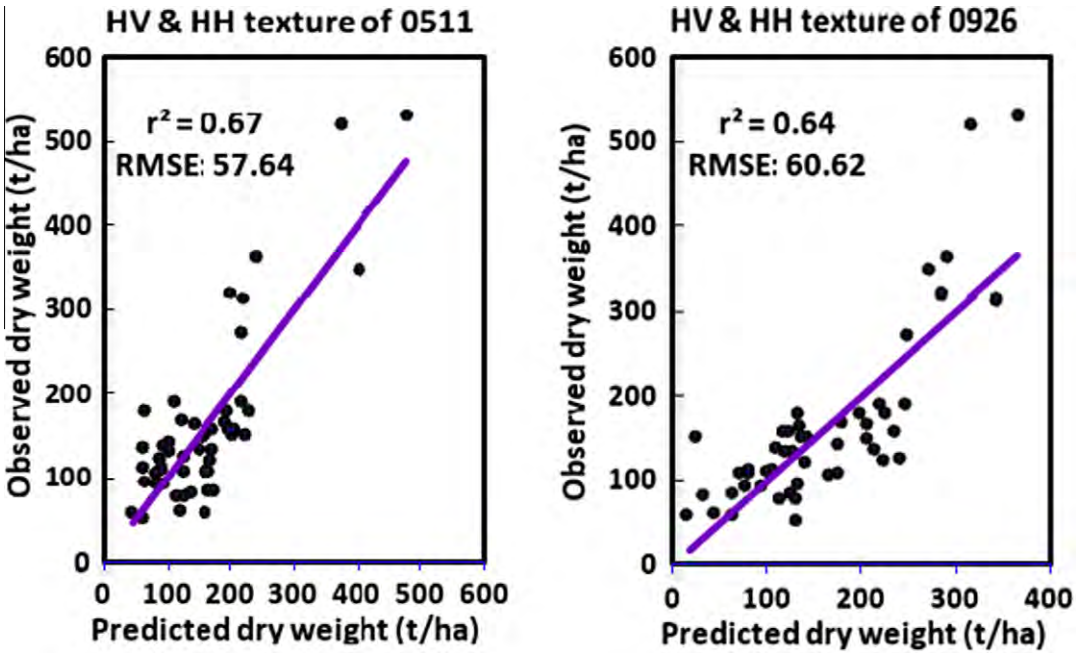

Fig. 13. Relationships between observed and model predicted biomass using texture parameters of HH & HV polarizations jointly.

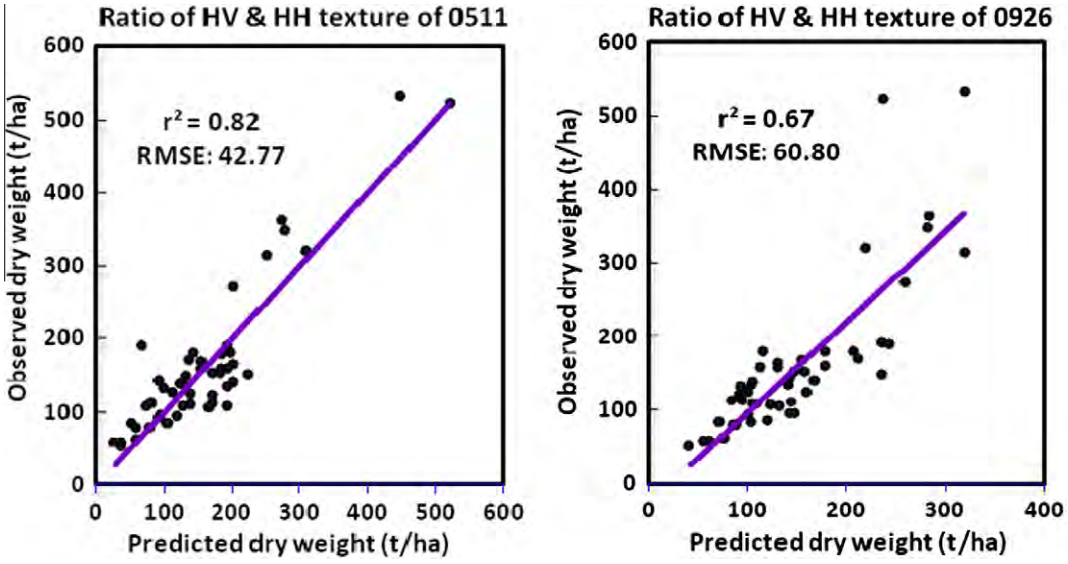

Fig. 14. Relationships between observed and model predicted biomass using ratio of texture parameters of HH & HV polarizations.

better than the result (adjusted $r^2 = 0.78$ & 0.68) obtained using a single-date ratio of HH and HV texture parameters (model 3 in Table 6). The model and intercept were significant, and multicollinearity effects were not noted. The RMSE (37.43) was lower than the model (RMSE 42.77 t/ha) for the corresponding single-date texture image ratio and the relationship between the observed and model-predicted biomass (Fig. 17) was also stronger than for any previous processing. This result confirms previous findings (Kurvonen et al., 1999) that averaging of several images can reduce the RMSE and improve biomass estimation.

In addition to the two-date texture parameters, we also investigated ratio combinations of single and two date texture parameters (Section 3.5.4 b). Thus it was possible to improve biomass estimation even further, and very promising results (adjusted $r^2 = 0.87$and0.90) were obtained (models 2 and 3 in Table 7). The best result (adjusted $r^2 = 0.90$) was obtained from the joint texture ratio-2 (model 3 in Table 7) with nine texture ratio variables (GLDV_Mean_9x9p + Homogeneity_5 × 5p + Amplitude Image + Kurtosis_5 × 5 + Normalized Coefficient of Variation_11 × 11p + Skewness_11 × 11p + Contrast_5 × 5 + VL_3 × 3 + GLDV Entropy_9 × 9). The model and intercept were significant and multicollinearity effects were minimal or absent, as all indicators (Tol, VIF, EV and CI) for multicollinearity effects were far below the predefined thresholds. The relationship between the observed and model predicted biomass (Fig. 16) appeared robust, as all plots including both low and high biomass were very close to the fit line resulting in a very low RMSE (28.58 t/ha). The result (adjusted $r^2 = 0.90$ and RMSE = 28.58 t/ha) is considerably better than for all previous processing steps in this research, and is much better than other results reported in the literature using L-band SAR in such a high biomass situation.

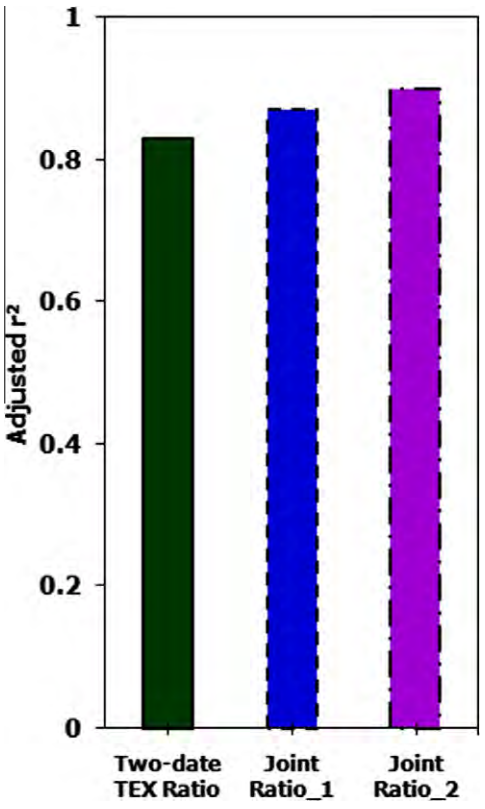

Fig. 15. Performance of biomass estimation using two-date texture parameters ratio and single-twodate texture parameters ratio combinations.

5. Validation performance

The results of the model validation are presented in Figs. 18–23 for two-date texture ratio (model 1 in Table 7), joint texture ratio-1 (model 2 in Table 7) and joint texture ratio-2 (model 3 in Table 7) respectively. Overall, the performances of the validation showed that the proposed three models in Section 4.4 were stable and can be used to predict forest biomass reasonably using independent field data though the performance was different among the three models.

The adjusted r^2 and RMSE of the model using the two-date texture ratio (model 1 in Table 7) was 0.83 and 37.43 t/ha respectively, and the adjusted r^2 (from 0.80 to 0.84) and RMSE (from 35.11 to 37.81 t/ha) computed for the training data using the LOO-CV method were similar however slightly worse than the original model (model 1 in Table 7). However, the overall validation accuracy (adjusted $r^2 = 0.78$ and RMSE = 47.93 t/ha) (Fig. 18) was worse than the original proposed model (adjusted $r^2 = 0.83$ and RMSE = 37.43 t/ha). Although the validation accuracy was worse

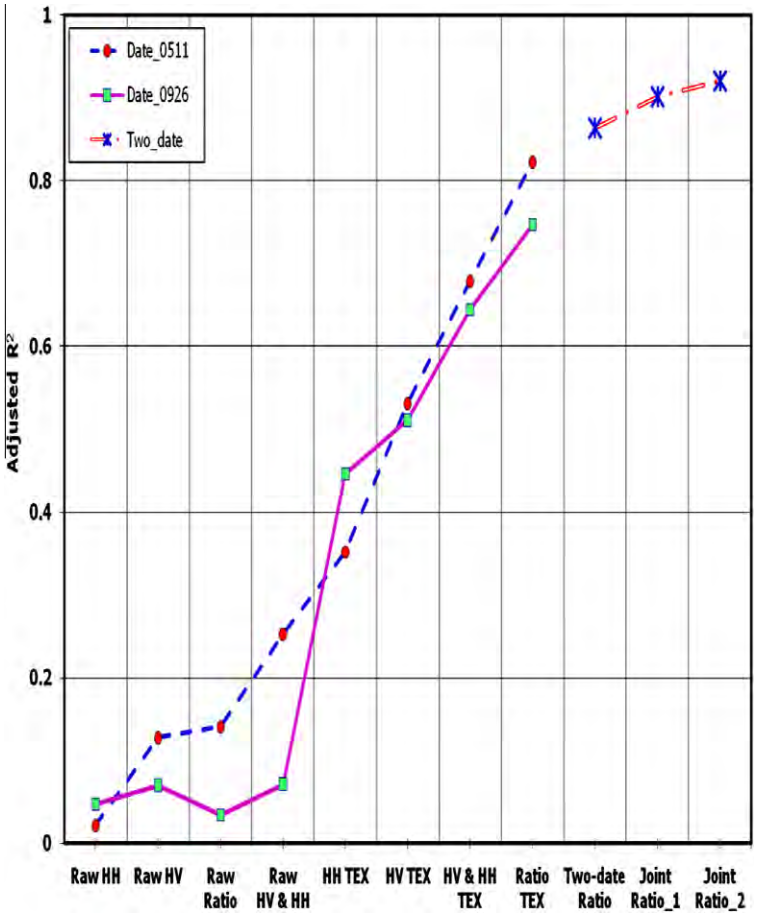

Fig. 16. Change in performance of biomass estimation among the all processing.

than the model accuracy, the accuracy was still reasonable considering the field biomass and number of sample size used for the development of a generalized model for biomass estimation in diversified forest conditions. In order to test the stability of the model and validation process, a comparison was made between the error (residual) of all points using the original proposed model and the error (residual) of all data points for the LOOCV. The result (Fig. 19) shows that the errors of the original model and of the validation data set were normally distributed and were strongly correlated with each other ($r^2 = 0.99$). Thus the same pattern of errors was observed in both the model and in the validation data points, although the magnitude of error was greater in the later. Therefore, the proposed model (model 1 in Table 7) could be considered to be stable and could be used for the estimation of forest biomass with an accuracy of ±47.93 t/ha.

The results of validation of the forest biomass estimation model using joint texture ratio 1 (model 2 in Table 7) were very similar to the two-date texture ratio (model 1 in Table 7). The adjusted r^2 (0.87) and RMSE (31.75 t/ha) of the original model (model 2 in Table 7) was more or less similar to the adjusted r^2 (from 0.84 to 0.89) and RMSE (from 29.19 to 32.07 t/ha) computed for the training data using LOOCV. The overall validation accuracy (adjusted $r^2 = 0.84$ and RMSE = 41.46 t/ha) (Fig. 20) was worse than the original model accuracy (adjusted $r^2 = 0.87$ and RMSE = 31.75 t/ha) but promising considering the high biomass level. However, the validation accuracy (adjusted $r^2 = 0.84$ and RMSE = 41.46 t/ha) of this model (model 2 in Table 7) was higher than the validation accuracy (adjusted $r^2 = 0.78$ and RMSE = 47.93 t/ha) of model 1 (Table 7). The errors (residuals) of both the original model and the validation data points were found to be distributed normally (Fig. 21), and there was a strong relationship ($r^2 = 0.99$) between them (Fig. 21). This indicates that the proposed model for forest biomass estimation using the joint texture ratio-1 (model 2 in Table 7) was stable and it performed better than the two-date texture ratio (model 1 in Table 7). This model has the ability to predict forest biomass using independent field data with an accuracy of ±41.46 t/ha.

The validation accuracy (adjusted $r^2 = 0.88$ and RMSE = 35.69 t/ha) (Fig. 22) of the proposed model (model 3 in Table 7) of forest biomass estimation using the joint texture ratio-2 model was higher than the validation accuracy of the other two models (for model 1 adjusted $r^2 = 0.78$ and RMSE = 47.93 t/ha, and for model 2 adjusted $r^2 = 0.84$ & RMSE = 41.46 t/ha). However, the validation accuracy (adjusted $r^2 = 0.88$ and RMSE = 35.69 t/ha) was worse than the model accuracy (adjusted $r^2 = 0.90$ and RMSE = 28.58 t/ha). But the difference in accuracy was very small (adjusted $r^2 = 0.02$ and RMSE = 7.16 t/ha) compared to the other two models (adjusted r^2 difference for model 1 = 0.4 and model 2 = 0.05). Similar to the other two models (model 1 and 2 in Table 7), errors of both the model and the validation data points were normally distributed (Fig. 23) and very strongly correlated with each other (Fig. 23). The lower difference in accuracy between model and validation, and the strong relationships between the model and validation error indicated that the model using joint texture ratio-2 (model 3 in Table 7) for forest biomass estimation was robust and outperformed the other two models (model 1 and 2 in Table 7), and has potential for the forest biomass estimation with an accuracy of ±35.69 t/ha.

Table 7
Results obtained from two-date dual polarization texture parameter combinations.

Data	Model fitting parameters				Fitting parameters for intercept and variables							
	r^2	r^2_{adj}	RMSE (t/ha)	p-Level	Variables name & intercept	B	Std. Err. of B	p-Level	Tol	VIF	EV	CI
Model 1: Two-date ratio of dual polarization texture parameters	0.86	0.83	37.43	.0005	Intercept	561.70	54.16	0.0005			4.12	1.000
					Kurtosis_3 × 3p	−39.18	5.32	0.0005	0.94	1.06	1.76	1.53
					Amplitude Image_p	−701.93	98.15	0.0005	0.65	1.53	1.20	1.85
					Skewness_5 × 5p	−2.49	0.82	0.0041	0.76	1.32	0.92	2.12
					Homogeneity_5 × 5p	19.04	4.79	0.0002	0.46	2.16	0.66	2.50
					VI_11 × 11p	68.39	6.66	0.0005	0.34	2.94	0.62	2.57
					Skewness_11 × 11p	−6.90	1.49	0.0003	0.28	3.55	0.34	3.48
					Kurtosis_11 × 11p	−15.49	3.86	0.0002	0.27	3.71	0.22	4.33
					Angular Second Moment_5 × 5p	−15.50	4.80	0.0024	0.49	2.03	0.15	5.25
					GLDV Entropy_3 × 3p	−11.72	4.05	0.0061	0.75	1.33	0.01	26.66
Model 2: Two-date joint texture ratio-1	0.90	0.87	31.75	.0005	Intercept	79.52	28.55	0.0082			5.22	1.00
					GLDV Entropy_9 × 9p	−57.85	23.95	0.0204	0.28	3.64	1.91	1.65
					Inverse Difference _7 × 7p	−39.81	9.96	0.0002	0.29	3.41	1.52	1.85
					Mean_9 × 9p	−161.86	31.62	0.0009	0.51	1.96	0.90	2.41
					Kurtosis_5 × 5p	−31.25	3.86	0.0005	0.59	1.68	0.50	3.24
					Skewness _5 × 5	2.83	0.87	0.0024	0.44	2.28	0.40	3.62
					Normalized Coefficient of Variation_11 × 11p	100.64	8.68	0.0005	0.25	4.01	0.24	4.64
					Skewness_11 × 11p	−13.93	1.34	0.0005	0.26	3.86	0.16	5.74
					Variance_3 × 3p	−14.41	2.06	0.0005	0.38	2.64	0.07	8.47
					Inverse Difference _7 × 7	43.41	7.60	0.0001	0.35	2.88	0.05	10.31
					Mean Dev. from Mean _3 × 3	5.99	2.36	0.0151	0.48	2.07	0.02	16.50
Model 3: Two-date joint texture ratio-2	0.92	0.90	28.58	.0005	Intercept	425.73	25.07	0.0005			4.65	1.00
					GLDV_mean_9 × 9p	22.02	7.10	0.0035	0.37	2.67	1.70	1.66
					Homogeneity_5 × 5p	27.61	3.67	0.0005	0.46	2.18	1.22	1.96
					Amplitude Image	−462.39	47.68	0.0005	0.67	1.49	1.02	2.13
					Kurtosis_5 × 5	−18.34	2.18	0.0005	0.82	1.22	0.54	2.93
					Normalized Coefficient of Variation_11 × 11p	59.80	5.71	0.0005	0.46	2.20	0.41	3.38
					Skewness _11 × 11p	−8.57	0.93	0.0005	0.42	2.39	0.22	4.60
					Contrast_5 × 5	12.86	1.81	0.0005	0.23	4.37	0.15	5.64
					VL_3 × 3	−15.60	2.49	0.0005	0.45	2.24	0.07	8.09
					GLDV Entropy_9 × 9	−43.21	12.98	0.0018	0.25	3.96	0.02	17.44

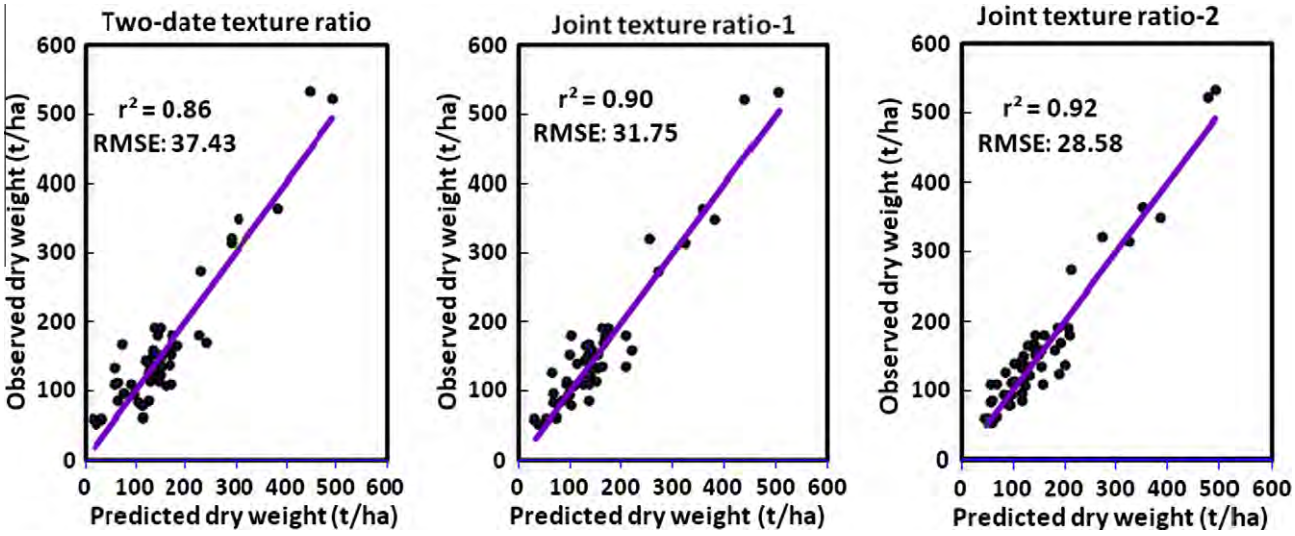

Fig. 17. Relationships between observed and model predicted biomass using the ratio of two-date texture parameters and combination of single-two date ratio combinations.

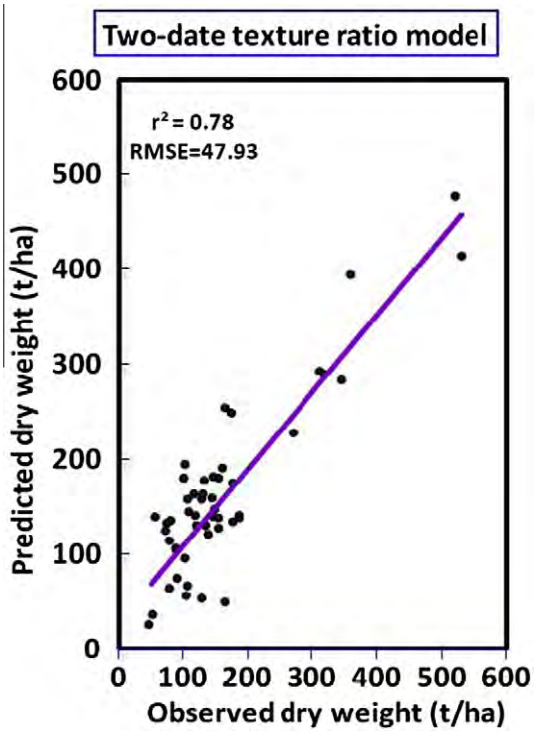

Fig. 18. Relationships between observed and predicted values for validation using LOOCV.

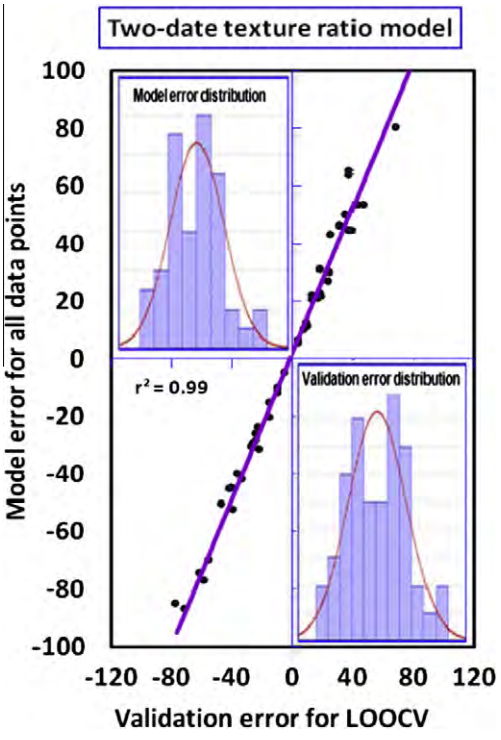

Fig. 19. Relationships and distribution of model error and validation error using LOOCV.

6. Discussion and conclusion

A wide range of results (adjusted r^2 from 0.22 to 0.90) was obtained from the biomass modeling using four different processing steps with the two-date PALSAR dataset. Performance improved with the number of processing steps (Fig. 16) and about 88% validation accuracy with an RMSE $\pm$ 35.69 t/ha at step 4 was obtained. No such result has so far been reported in the literature using L-band SAR in such high biomass conditions and this result suggests there is great potential for the use of PALSAR in biomass estimation.

The performance obtained using different combinations of intensity data processing was low and inconsistent. This is in agreement with other researchers (Dobson et al., 1992; Rignot et al., 1994; Foody et al., 1997) who found that the raw backscattering coefficient does not correlate strongly with biomass because of speckle noise and saturation problem. Although the ratio of backscattering has often been found effective (Dobson et al., 1995; Ranson and Sun, 1994; Harrell et al., 1997), our results did not show this, probably because of the high biomass in this study area which is far beyond the reported saturation point of L-band SAR.

Texture parameters of HH and HV polarization data were found to be more robust than raw SAR data, and HV texture polarization more effective than HH texture polarization. The observed improvement using texture parameters is not completely new

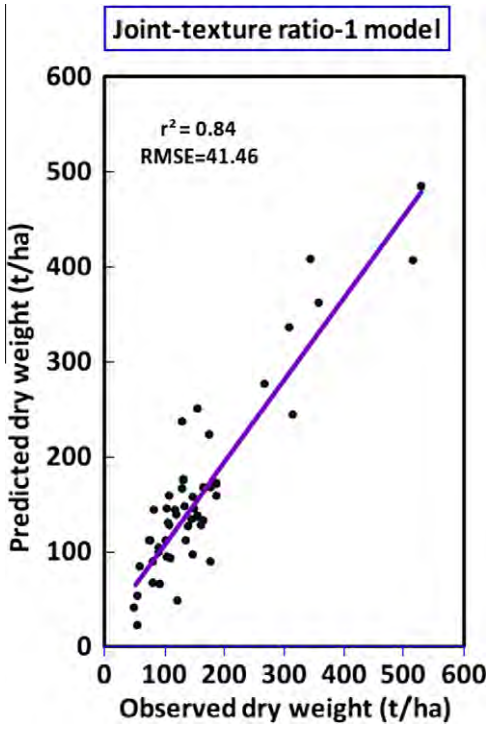

Fig. 20. Relationships between observed and predicted value of validation using LOOCV.

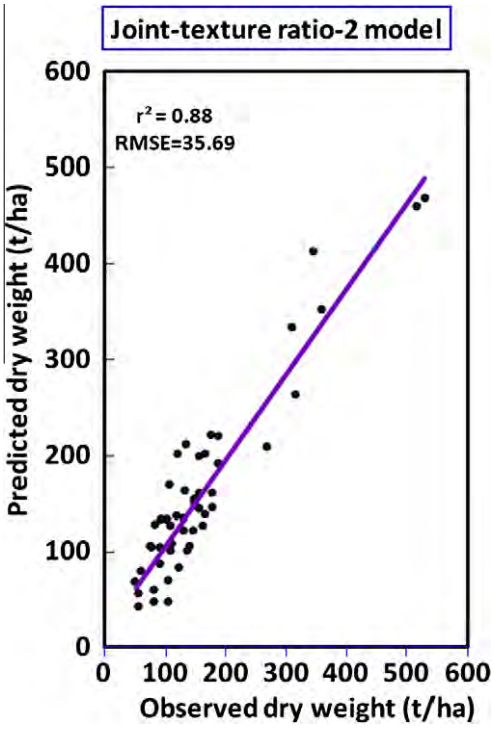

Fig. 22. Relationships between observed and predicted values for validation using LOOCV.

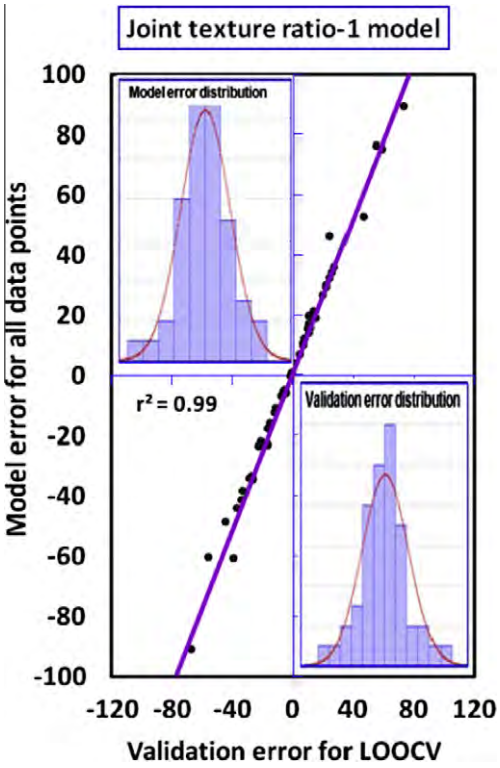

Fig. 21. Relationships and distribution of model error and validation error using LOOCV.

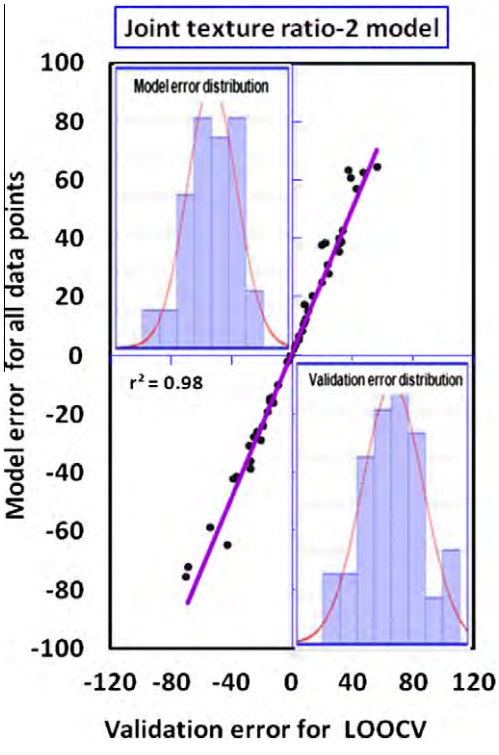

Fig. 23. Relationships and distribution of model error and validation error using LOOCV.

and agrees with previous research (Luckman et al., 1997; Salas et al., 2002; Kuplich et al., 2005; Champion et al., 2008). Also, the better performance of HV than HH polarization SAR data reported in many studies (Rauste et al., 1994; Ranson et al., 1995; Kasischke et al., 1995; Mougin et al., 1999; Collins et al., 2009) is supported by our findings.

The use of both polarization texture parameters jointly in the model with and without ratio improved the performance of biomass estimation compared to any single polarization texture, probably as different polarizations provide complementary information, as observed by Kasischke et al. (1997) and Rignot et al. (1994), whereas the addition of texture parameters to this information is able to reduce the inherent noise in the SAR data. However, the texture parameter ratio model (in the form of HV/HH) was found to be more effective than the model without ratio. This is probably because ratio images combine both the complementary information from their use as independent parameters without ratio, as well reduce topographic effects and forest type structural differences. As a result the ratio is able to further increase the performance from dual polarization texture parameters.

The highest performance of biomass estimation was reached using the ratio of two-date dual polarization texture parameters and a combination of single and two-date ratios together as independent parameters in the model. This improvement in principle agrees with previous findings for multi-date SAR research (Kurvonen et al., 1999; Fransson and Israelsson, 1999) that the use of several different dates of SAR by averaging or other means can provide more reliable results than a single SAR image, by reduction of speckle noise and other random errors. In summary, the improvement of results using the combination of single and two-date dual polarization texture image ratios compared to all previous processing steps can be explained by a combination of complementarities in the datasets and minimization of error due to image noise.

It should be noted that in almost all processing steps the date 2 (11 May, 2008) image provided better results than date 1 (26 September, 2009). Since the forest type in the study area is evergreen, little structural change would be expected between May and September. However, climate data showed that two to three days before the date 1 (26 September, 2008) image acquisition very heavy rainfall (in some places more than 150 mm) was observed, but only slight rainfall (10–15 mm) was recorded before date 1 (11 May, 2008) image acquisition.

Although rainfall occurred before both of the image dates, very heavy rainfall before date 1 (26 September, 2008) made the surface very moist. Despite L-band SAR may be less sensitive to soil moisture than C-band, we assume that the differences in performance was due to influence of the surface moisture conditions, and this agrees with other research (Harrell et al., 1995) which reported poor relationships between ERS-1 data and tree biomass during early summer when snow melt and precipitation make the surface very moist, but increasing backscatter is observed with increasing biomass in late winter when the surface dries out.

The LOOCV method proved to be promising and validation accuracies (adjusted r^2) of 0.78, 0.84 and 0.88 were obtained compared to the model accuracies (adjusted r^2) of 0.83, 0.87 and 0.90 from the proposed three models (two-date ratio, joint ratio-1 and joint ratio-2, respectively). The difference between the models and LOOCV validation accuracy was not very high and it was acceptable considering the sample size and diversified forest condition.

This paper presents techniques which are able to achieve high performance of biomass estimation (adjusted $r^2 = 0.90$ for model and 0.88 for validation) in a study area where biomass levels are as high as 500 t/ha, whereas previous reported saturation levels have been given as 60–70 t/ha for L-band SAR. This very strong performance was achieved by combining four strategies which had already been used or suggested individually by other researchers. These include the use of (i) a longer wavelength SAR sensor, (ii) texture measurements, (iii) dual polarization SAR data and (iv) two-date SAR data. The good results obtained from this research are actually the outcome of appropriate image selection and processing techniques together.

7. Recommendations for future work

Different types of forest biomass estimation models were proposed and validated using the two-date dual polarizations of PALSAR data. The proposed techniques have potential for forest biomass estimation and may be used in similar field situations although we believe that other texture combinations may give better results in other forest conditions, as texture measurement depends on the biophysical and environmental conditions of the area of interest. Thus researchers may need to select others combinations of texture parameters for their study area. However, the processing presented here can be used as templates for future work.

This research was based on dual polarization SAR data and the relationships between SAR and ground-truth data were established using stepwise multiple regression method. However, although our data is not fully polarimetric, there are several other useful methods such as polarimetric interferometric (PolInSAR) model inversion techniques for forest parameter estimation and the associated 'Random Volume Over Ground' class of models (Mette et al., 2004; Cloude and Papathanassiou, 2003; Papathanassiou and Cloude, 2001; Brandfass et al., 2001) which should be taken into account in future studies, because PolInSAR processing does not require assumptions concerning the relationship between observables and parameters (e.g. a linear relationship in this study) and can be applied in the absence of ground-truth data.

Acknowledgement

The authors would like to acknowledge GRF Grant PolyU 5253/10E from the Hong Research Grants Council and FAVF-4D059 from the Universiti Teknologi Malaysia (UTM). The authors are also very thankful to the Japan Aerospace Exploration Agency for the ALOS images, under ALOS agreement no. 376.

References

Arevalo, C.B.M., Volk, T.A., Bevilacqua, E., Abrahamson, L., 2007. Development and validation of aboveground biomass estimations for four Salix clones in central New York. Biomass and Bioenergy 31 (1), 1–12.

Austin, J.M., Mackey, B.G., Van Niel, K.P., 2003. Estimating forest biomass using satellite radar: an exploratory study in a temperate Australian Eucalyptus forest. Forest Ecology and Management 176 (1-3), 575–583.

Baraldi, A., Parmiggiani, F., 1995. An investigation of the texture characteristics associated with gray level cooccurrence matrix statistical parameters. IEEE Transactions on Geoscience and Remote Sensing 33 (2), 293–304.

Belsley, D.A., 1990. Conditioning Diagnostics, 1st ed. John Willy, New York.

Belsley, D.A., Kuh, E., Welsch, R.E., 1980. Regression Diagnostics: Identifying Influential Data and Sources of Collinearity, 1st ed. John Wiley, New York.

Brandfass, M., Hofmann, C., Mura, J.C., Papathanassiou, K.P., 2001. Polarimetric SAR interferometry as applied to fully polarimetric rain forest data. In: Proc. of Geoscience and Remote Sensing Symposium IGARSS'01, vol. 6, pp. 2575-2577.

Brown, S., 1997. Estimating Biomass and Biomass Change of Tropical Forests: A Primer. FAO – Food and Agriculture Organization of the United Nations, Rome, 1997 (FAO Forestry Paper – 134).

Brown, S., Gillespie, A.J.R., Lugo, A.E., 1989. Biomass estimation methods for tropical forests with applications to forest inventory data. Forest Science 35 (4), 881–902.

Castel, T., Guerra, F., Caraglio, Y., Houllier, F., 2002. Retrieval biomass of a large Venezuelan pine plantation using JERS-1 SAR data. Analysis of forest structure impact on radar signature. Remote Sensing of Environment 79 (1), 30–41.

Cawley, G.C., Talbot, N.L.C., 2004. Fast exact leave-one-out cross-validation of sparse least-squares support vector machines. Neural Networks 17 (10), 1467–1475.

Champion, I., Dubois-Fernandez, P., Guyon, D., Cottrel, M., 2008. Radar image texture as a function of forest stand age. International Journal of Remote Sensing 29 (6), 1795–1800.

Chen, D., Stow, D.A., Gong, P., 2004. Examining the effect of spatial resolution and texture window size on classification accuracy: an urban environment case. International Journal of Remote Sensing 25 (11), 2177–2192.

Cloude, S.R., Papathanassiou, K.P., 2003. Three-stage inversion process for polarimetric SAR interferometry. IEE Proceedings – Radar Sonar and Navigation 150 (3), 125–134.

Collins, J.N., Hutley, L.B., Williams, R.J., Boggs, G., Bell, D., Bartolo, R., 2009. Estimating landscape-scale vegetation carbon stocks using airborne multi-

frequency polarimetric synthetic aperture radar (SAR) in the savannahs of north Australia. International Journal of Remote Sensing 30 (5), 1141–1159.
Dekker, R.J., 2003. Texture analysis and classification of ERS SAR image for Map updating of urban areas in the Netherlands. IEEE Transactions on Geoscience and Remote Sensing 41 (9), 1950–1958.
Dell'Acqua, F., Gamba, P., 2003. Texture-based characterization of urban environments on satellite SAR images. IEEE Transactions on Geoscience and Remote Sensing 41 (1), 153–159.
Dobson, M.C., Ulaby, F.T., Le Toan, T., Beaudoin, A., Kasischke, E.S., Christensen, N.C., 1992. Dependence of radar backscatter on conifer forest biomass. IEEE Transactions on Geoscience and Remote Sensing 30 (2), 412–415.
Dobson, M.C., Ulaby, F.T., Pierce, L.E., Sharik, T.L., Bergen, K.M., Kellndorfer, J., Kendra, J.R., Li, E., Lin, Y.C., Nashashibi, A., Sarabandi, K., Siqueira, P., 1995. Estimation of forest biomass characteristics in northern Michigan with SIR-C/X-SAR data. IEEE Transactions on Geoscience and Remote Sensing 33 (4), 877–894.
Douglas, C.M., Peck, E.A., Vining, G.G., 2006. Introduction to Linear Regression Analysis, 4th ed. Wiley & Sons publication, New Jersey.
Foody, G.M., Boyd, D.S., Cutler, M.E.J., 2003. Predictive relations of tropical forest biomass from Landsat TM data and their transferability between regions. Remote Sensing of Environment 85 (4), 463–474.
Foody, G.M., Green, R.M., Curran, P.J., Lucas, R.M., Honzak, M., Do Amaral, I., 1997. Observations on the relationship between SIR-C radar backscatter and the biomass of regenerating tropical forests. International Journal of Remote Sensing 18 (3), 687–694.
Fransson, J.E.S., Israelsson, H., 1999. Estimation of stem volume in boreal forests using ERS-1 C- and JERS-1 L-band SAR. International Journal of Remote Sensing 20 (1), 123–137.
Haralick, R.M., Shanmugam, K., Dinstein, I., 1973. Texture features for image classification. IEEE Transactions on Systems, Man and Cybernetics 3 (6), 610–621.
Harrell, P.A., Bourgeau-Chavez, L.L., Kasischke, French, N.H.F., Christensen Jr., N.L., 1995. Sensitivity of ERS-1 and JERS-1 Radar data to biomass and stand structure in Alaskan boreal forest. Remote Sensing of Environment 54 (3), 247–260.
Harrell, P.A., Kasischke, E.S., Bourgeau-Chavez, L.L., Haney, E.M., Christensen Jr., N.L., 1997. Evaluation of approaches aboveground biomass in using SIR-C data. Remote Sensing of Environment 59 (2), 223–233.
Hese, S., Lucht, W., Schmullius, C., Barnsley, M., Dubayah, R., Knorr, D., Neumann, K., Riedel, T., Schroter, K., 2005. Global biomass mapping for an improved understanding of the CO_2 balance – the Earth observation mission Carbon-3D. Remote Sensing of Environment 94 (1), 94–104.
Hussin, Y.A., Reich, R.M., Hoffer, R.M., 1991. Estimating slash pine biomass using radar backscatter. IEEE Transactions on Geoscience and Remote Sensing 29 (3), 427–431.
Hyde, P., Dubayah, R., Walker, W., Blair, J.B., Hofton, M., Hunsaker, C., 2006. Mapping forest structure for wildlife habitat analysis using multi-sensor (LiDAR, SAR/InSAR, ETM+, Quickbird) synergy. Remote Sensing of Environment 102 (1-2), 63–73.
Hyde, P., Nelson, R., Kimes, D., Levine, E., 2007. Exploring LiDAR–RaDAR synergy – predicting aboveground biomass in a southwestern ponderosa pine forest using LiDAR, SAR and InSAR. Remote Sensing of Environment 106 (1), 28–38.
Imhoff, M.L., 1995. Radar backscatter and biomass saturation: ramification for global biomass inventory. IEEE Transactions on Geoscience and Remote Sensing 33 (2), 511–518.
Kasischke, E.S., Bourgeau-Chavez, L.L., Christensen Jr., N.L., Haney, E., 1994. Observations on the sensitivity of ERS-1 SAR image intensity to changes in aboveground biomass in young loblolly pine forests. International Journal of Remote Sensing 15 (1), 3–16.
Kasischke, E.S., Christensen, N.L., Bourgeau-Chavez, L.L., 1995. Correlating Radar backscatter with components of biomass in loblolly pine forests. IEEE Transactions on Geoscience and Remote Sensing 33 (3), 643–659.
Kasischke, E.S., Melack, J.M., Dobson, M.C., 1997. The use of imaging radars for ecological applications – a review. Remote Sensing of Environment 59 (2), 141–156.
Ketterings, Q.M., Coe, R., van Noordwijk, M., Ambagau, Y., Palm, C.A., 2001. Reducing uncertainty in the use of allometric biomass equations for predicting above-ground tree biomass in mixed secondary forests. Forest Ecology and Management 146 (1-3), 199–209.
Kuplich, T.M., Curran, P.J., 2003. Estimating texture independently of tone in simulated images of forest canopies. In: Proc. of XIth Brazilian Remote Sensing Symposium, pp. 2209–2216.
Kuplich, T.M., Curran, P.J., Atkinson, P.M., 2005. Relating SAR image texture to the biomass of regenerating tropical forest. International Journal of Remote Sensing 26 (21), 4829–4854.
Kurvonen, L., Pulliainen, J., Hallikainen, M., 1999. Retrieval of biomass in boreal forests from multitemporal ERS-1 and JERS-1 SAR data. IEEE Transactions on Geoscience and Remote Sensing 37 (1), 198–205.
Kutner, M.H., Nachtsheim, C.J., Neter, J., Li, W., 2005. Applied Linear Statistical Models, 5th ed. McGraw-Hill Companies, New York.
Le Toan, T., Beaudoin, A., Riom, J., Guyon, D., 1992. Relating Forest Biomass to SAR Data. IEEE Transactions on Geoscience and Remote Sensing 30 (2), 403–411.
Lu, D., 2005. Aboveground biomass estimation using Landsat TM data in the Brazilian Amazon. International Journal of Remote Sensing 26 (12), 2509–2525.
Lu, D., 2006. The potential and challenge of remote sensing-based biomass estimation. International Journal of Remote Sensing 27 (7), 1297–1328.
Lucas, R.M., Honza, K.M., Curran, P.J., Foody, G.M., Milne, R., Brown, T., Amaral, S., 2000. Mapping the regional extent of tropical forest regeneration stages in the Brazilian Legal Amazon using NOAA AVHRR data. International Journal of Remote Sensing 21 (15), 2855–2881.
Lucas, R.M., Mitchell, A.L., Rosenqvist, A., Proisy, C., Melius, A., Ticehurst, C., 2007. The potential of L-band SAR for quantifying mangrove characteristics and change: case studies from the tropics. Aquatic Conservation: Marine and Freshwater Ecosystem 17 (3), 245–264.
Luckman, A., Baker, J., Honzak, M., Lucas, R., 1998. Tropical forest biomass density estimation using JERS-1 SAR: seasonal variation, confidence limits, and application to image mosaics. Remote Sensing of Environment 63 (2), 126–139.
Luckman, A., Frery, A.C., Yanasse, C.C.F., Groom, G.B., 1997. Texture in airborne SAR imagery of tropical forest and its relationship to forest regeneration stage. International Journal of Remote Sensing 18 (6), 1333–1349.
Mette, T., Papathanassiou, K.P., Hajnsek, I., 2004. Biomass estimation from polarimetric SAR interferometry over heterogeneous forest terrain. In: Proc. of Geoscience and Remote Sensing Symposium, IGARSS '04, Anchorage, 20–24 September, pp. 511–514.
Mougin, E., Proisy, C., Marty, G., Fromard, F., Puig, H., Betoulle, L., Rudant, J.P., 1999. Multifrequency and multipolarization Radar backscattering from Mangrove frosts. IEEE Transactions on Geoscience and Remote Sensing 37 (1), 94–102.
Nelson, R.F., Kimes, D.S., Salas, W.A., Routhier, M., 2000. Secondary forest age and tropical forest biomass estimation using Thematic Mapper imagery. Bioscience 50 (5), 419–431.
Nyoungu, N.A., Tonye, E., Akono, A., 2002. Evaluation of speckle filtering and texture analysis methods for land cover classification from SAR images. International Journal of Remote Sensing 23 (9), 1895–1925.
Oliver, C.J., 1993. Optimum texture estimators for SAR clutter. Journal of Physics D: Applied Physics 26 (11), 1824–1835.
Oliver, C., Quegan, S., 2004. Understanding Synthetic Aperture Radar Images. SciTech Publication, Raleigh, N.C..
Overman, J.P.M., Witte, H.J.L., Saldarriaga, J.G., 1994. Evaluation of regression models for above-ground biomass determination in Amazon rainforest. Journal of Tropical Ecology 10 (2), 207–218.
Papathanassiou, K.P., Cloude, S.R., 2001. Single baseline polarimetric SAR interferometry. IEEE Transactions on Geoscience and Remote Sensing 39 (11), 2352–2363.
Podest, E., Saatchi, S., 2002. Application of multiscale texture in classifying JERS-1 radar data over tropical vegetation. International Journal of Remote Sensing 23 (7), 1487–1506.
Ranson, K.J., Sun, G., Lang, R., Chauhan, N., Cacciola, R., Kilic, O., 1997. Mapping of boreal forest biomass from spaceborne synthetic aperture radar. Journal of Geophysical Research 102 (D24), 29599–29610.
Ranson, K.J., Saatchi, S., Sun, G., 1995. Boreal forest ecosystem characterization with SIR-C/XSAR. IEEE Transactions on Geoscience and Remote Sensing 33 (4), 867–876.
Ranson, K.J., Sun, G., Kharuk, V.I., Kovacs, K., 2001. Characterization of forests in Western Sayani Mountains, Siberia from SAR data. Remote Sensing of Environment 75 (c), 188–200.
Ranson, K.J., Sun, G., 1994. Mapping biomass of a northern forest using multifrequency SAR data. IEEE Transactions on Geoscience and Remote Sensing 32 (2), 388–396.
Rauste, Y., Hame, T., Pulliainen, J., Heiska, K., Hallikainen, M., 1994. Radar-based forest biomass estimation. International Journal of Remote Sensing 15 (14), 2797–2808.
Rignot, E., Way, J., Williams, C., Viereck, L., 1994. Radar estimates of aboveground biomass in boreal forests of interior Alaska. IEEE Transactions on Geoscience and Remote Sensing 32 (5), 1117–1124.
Rignot, E.J., Zimmermann, R., van Zyl, J.J., 1995. Spaceborne applications of P band imaging Radars for measuring forest biomass. IEEE Transactions on Geoscience and Remote Sensing 33 (5), 1162–1169.
Rosenqvist, Å., Milne, A., Lucas, R., Imhoff, M., Dobson, C., 2003. A review of remote sensing technology in support of the Kyoto protocol. Environmental Science and Policy 6 (5), 441–455.
Salas, W.A., Ducey, M.J., Rignot, E., Skole, D., 2002. Assessment of Jers-1 SAR for monitoring secondary vegetation in Amazonia: I. Spatial and temporal variability in backscatter across chrono-sequence of secondary vegetation stands in Rondonia. International Journal of Remote Sensing 23 (7), 1357–1379.
Santos, J.R., Pardi Lacruz, M.S., Araujo, L.S., Keil, M., 2002. Savanna and tropical rainforest biomass estimation and spatialization using JERS-1 data. International Journal of Remote Sensing 23 (7), 1217–1229.
Santos, J.R., Freitas, C.C., Araujo, L.S., Dutra, L.V., Mura, J.C., Gama, F.F., Soler, L.S., Sant'Anna, S.J.S., 2003. Airborne P-band SAR applied to the aboveground biomass studies in the Brazilian tropical rainforest. Remote Sensing of Environment 87 (4), 482–493.
Shi, J., Dozier, J., 1997. Mapping seasonal snow with SIR-C/X-SAR in mountainous areas. Remote Sensing of Environment 59 (2), 294–307.
Steininger, M.K., 2000. Satellite estimation of tropical secondary forest above-ground biomass: data from Brazil and Bolivia. International Journal of Remote Sensing 21 (6-7), 1139–1157.
Sun, G., Ranson, K.J., Kharuk, V.I., 2002. Radiometric slope correction for forest biomass estimation from SAR data in the western Sayani Mountains, Siberia. Remote Sensing of Environment 79 (2-3), 279–287.
Townsend, P.A., 2002. Estimating forest structure in wetlands using multitemporal SAR. Remote Sensing of Environment 79 (2-3), 288–304.
Tsolmon, R., Tateishi, R., Tetuko, J.S.S., 2002. A method to estimate forest biomass and its application to monitor Mongolian Taiga using JERS-1 SAR data. International Journal of Remote Sensing 23 (22), 4971–4978.

Ulaby, F.T., Kouyate, F., Brisco, B., Williams, T.H.L., 1986. Textural information in SAR images. IEEE Transactions on Geoscience and Remote Sensing 24 (2), 235–240.

Unser, M., 1986. Sum and difference histogram for texture classification. IEEE Transactions on Pattern Analysis and Machine Intelligence PAMI-8 (1), 118–125.

Wu, S., 1987. Potential application of multipolarization SAR for pine-plantation biomass estimation. IEEE Transactions on Geoscience and Remote Sensing 25 (3), 403–409.

Zheng, D., Rademacher, J., Chen, J., Crow, T., Bresee, M., LE Moine, J., Ryu, S., 2004. Estimating aboveground biomass using Landsat 7 ETM+ data across a managed landscape in northern Wisconsin, USA. Remote Sensing of Environment 93 (3), 402–411.